Chapter 11

All-Oxide Solar Cells

Theodoros Dimopoulos
AIT Austrian Institute of Technology, Center for Energy, Vienna, Austria

11.1 INTRODUCTION—CHALLENGES FOR LARGE-SCALE PV DEPLOYMENT

In 2004, in his testimony before the U.S. Senate Committee on Energy and Natural Resources, the Nobel laureate Richard E. Smalley stated that "energy is the single most important challenge facing humanity today" and that "for worldwide peace and prosperity, it must be cheap." Indeed, the intensive combustion of fossil fuels as our primary energy source led to an unprecedented increase of greenhouse gas emissions in the last decades, resulting in global warming, with dire consequences for the planet.

The CO_2 concentration data gathered form the ice-core and Mauna Loa observatory (the latter known as the "Keeling curve") clearly show that, while the concentration in the atmosphere varied periodically between 180 and 280 ppm the last 800,000 years, a dramatic continuous increase is marked since the 1950s, reaching the record value of 407 ppm in 2016. As a consequence, according to the NASA global climate change research, the average land-ocean temperature has risen by 0.87°C in 2015, relative to the 1951–80 baseline. Global warming causes the sea level to rise, patterns and intensity of weather phenomena to change, the Arctic ice to retreat, extended periods of drought to occur, etc. To mitigate the climate change, we need to drastically reduce the use of fossil fuels, deploying renewable energy sources quickly and on a large scale.

The deployment of renewables will also lead to a "democratization" of the energy supply and consumption. In a world where the population and energy demand are rapidly increasing, we have to ensure that everyone has access to plentiful cheap energy. Until now, only few countries and companies control the worldwide energy supply by controlling the fossil fuel reserves. With renewables, a decentralized energy production can materialize, through which individuals and communities even in the poorest regions of the world can independently serve their energy needs. But is it possible to cover the worldwide energy demand by renewables?

The Future of Semiconductor Oxides in Next-Generation Solar Cells. https://doi.org/10.1016/B978-0-12-811165-9.00011-9

According to the International Energy Agency (IEA), from the world total primary energy supply in 2014, which summed up to 13,699 MTOE (megatons of oil equivalent), 81.1% came from fossil fuels (oil, coal, and natural gas), 10.3% from biofuel and waste, 4.8% from nuclear, 2.4% from hydro and 1.4% from other sources, like solar, wind, and geothermal [1]. The contribution of renewables to the energy mix is therefore extremely small. In his article "Powering the planet," Nathan S. Lewis demonstrated that from all the carbon-neutral energy sources, solar photovoltaics is the only source capable of covering the world's energy demand [2]. Indeed, the sun provides 120,000 TW of power at any moment, which practically covers the annual worldwide energy demand in just 1 h. To make a significant impact in the energy landscape, PV needs to be deployed on a multi-TW_p (terawatt-peak) scale.

This level of deployment is far from being reached, even if the PV market has grown impressively in the last decade. From 2005 to 2015, the worldwide commissioned PV capacity jumped from 5 to 229 GW_p, i.e., a forty-five-fold market growth. Nearly 51 GW_p were installed in 2015, and the projected installed capacity by 2020 is most likely 613 GW_p [3]. However impressive this growth may be, it is still dwarfed by the multi-TW_p target-capacity. From the technology point of view, crystalline Si (c-Si) PV represents about 90% of the installed capacity. The rest 10% is shared by the two dominant thin film technologies, based on the cadmium telluride (CdTe) and the copper indium gallium di-selenide (CIGS) absorbers. State-of-the-art cell efficiencies, at laboratory level, reach above 20% for these technologies, while CdTe module efficiencies have reached recently over 16% in mass production, a level comparable to the crystalline silicon modules.

An important question for TW_p deployment is whether we have enough material resources at hand. Wadia et al. [4] explored material limits for PV expansion by examining the dual constraints of material supply and least cost-per-watt for 23 inorganic semiconductors as active solar absorbers. Their analysis was based on the annual production levels and known economic reserves of the elements composing the absorber, on the necessary absorber thickness given by its light absorption coefficient and its electricity generation potential, given by the thermodynamic upper limit of its efficiency. Aspects like stability, defects, toxicity, and ease of manufacturing were not taken into account. The result of this investigation was that the commercial CdTe and CIGS technologies are not able to reach the multi-TW target without facing problems of materials availability, mostly due to the scarcity of Te and Ga.

In a recent work from Jean et al. [5], material requirements were determined for a number of PV technologies based on c-Si, amorphous Si (a-Si), CIGS, CdTe, Pb-perovskite, organic PV (OPV) and quantum dots. Their analysis explored the scenarios that a technology covers 5%, 50%, or 100% of the global electricity demand in 2050, estimated at 1.25, 12.5, and 25 TW_p of installed PV. Based on the current production of each material, the authors estimated the time needed to extract the corresponding amount of material for each deployment

level. To meet 100% of the demand with c-Si and a-Si solar cells would require respectively 6 years and 2 months of current Si production. So, materials availability is not an issue for Si. The corresponding times for Pb-perovskite and OPV are about 3 years and few minutes, respectively. On the other hand, materials availability seems a serious issue for CdTe and CIGS technologies, as more than 1000 years of Te production and about 500 years of Ga would be required for 100% deployment. Again, the long-term stability and materials toxicity issues are not taken into account in this analysis, but are critical for increased PV deployment.

The next important question is whether solar PV is competitive in terms of cost-per-watt to fossil-fuel-run power plants. The answer is affirmative. Today, the cost of utility-scale solar power is lower than conventional power plants, and the electricity from distributed PV is cheaper than the retail grid electricity price for an increasing number of countries. Illustratively, in a recent solar tender in Dubai, the bidding price was as low as 2.99 US cents per kWh. Although this price is influenced by national conditions, it outcompetes most fossil-fuel plants today [3].

The production processes have a key role in further reducing the cost-per-watt of PV. High throughput, roll-to-roll processing is, to this end, highly relevant. This is especially true when it is combined with non-vacuum techniques, featuring low capital expenditure and maintenance costs. Materials which are easily manufactured with these techniques have a competitive edge for TW-scale deployment. According to Unold & Schock [6], these would be thin film, polycrystalline materials with direct bandgap that matches well the solar spectrum and with high tolerances to deviations of stoichiometry and to the presence of impurities. Thin film PV also offers new possibilities for implementation in the built environment (e.g., in building façades), as they can be fabricated on flexible and low-cost substrates (e.g., plastic foils, metallic sheets), they are lightweight and can operate at high efficiency at nonoptimal light angles (e.g., for vertical installation in building façades).

In the quest to design thin film solar cells with improved efficiency, some fundamental criteria of solar cell operation need to be taken into account, and they are reviewed in the following section.

11.2 CRITERIA FOR EFFICIENT THIN FILM SOLAR CELLS

The photoconversion efficiency of single-junction solar cells is determined by the following loss mechanisms: (i) Photons with energies lower than the bandgap are not absorbed. (ii) Photogenerated electron-hole pairs are subject to radiative recombination. (iii) Photon energy above the bandgap is lost by carrier thermalization to the conduction band minimum and the valence band maximum. (iv) Nonradiative carrier recombination. (v) Carrier transport losses due to finite minority carrier mobility. (vi) Optical reflections. The first three mechanisms are included in the Shockley-Queisser detailed balance limit model [7],

which gives a maximum of 33.7% efficiency for a 1.34 eV bandgap absorber under AM1.5 spectrum light. The last three types of losses considerably reduce the cell efficiency from the level predicted by the detailed balance model, and therefore have to be carefully addressed in the cell design.

A typical thin film solar cell has the following components: (i) A metallic electrode, which provides an ohmic contact to the absorber layer. (ii) A *p*- or *n*-type absorber, with *p*-type preferred as it offers higher minority carrier mobilities. Ideally, the absorber should have a direct bandgap of ~1.4 eV for a single junction cell. Nevertheless, bandgap values from 1.0 eV to more than 2.0 eV are useful, depending on the solar cell design and application. The absorber should have a large absorption coefficient, α, and thickness $d > 2/\alpha$, in order to absorb most of the light. In addition, the minority carrier diffusion length, L, should be larger than $1/\alpha$, so that the carriers can reach the electrodes without being recombined. To keep recombination losses low, impurity levels must be kept low, and the absorber grains must be sufficiently large. (iii) A "buffer" layer with the opposite type of conductivity than the absorber forms the heterojunction. The buffer layer needs to have a significantly larger bandgap than the absorber and be sufficiently thin, so that the light absorption in the buffer layer is minimal. It should also have a proper energy band alignment with the absorber, to guarantee a high open circuit voltage (V_{oc}) for the device. (iv) A transparent conductive electrode, which ideally forms an ohmic contact with the buffer layer. Apart from these basic cell components, ultra-thin interfacial layers are widely used to improve the energy band alignment to the anode or cathode.

11.3 OXIDES IN THE CURRENT PV LANDSCAPE

Oxides are indispensable and most versatile components of inorganic, organic, and hybrid perovskite solar cells. They are employed as: (i) transparent contacts; (ii) anode or cathode interfacial layers for energy band alignment; (iii) nanostructures and porous scaffolds for light management, enhanced carrier collection efficiency, and active area enhancement; and (iv) active solar absorbers. This versatility stems from their rich electronic properties and their ability to be processed with a variety of vacuum- and solution-based, low-cost techniques, in the form of films or nanostructures. On top of that, many of these oxides are composed of abundant, nontoxic elements.

The most widespread application of metal oxides is as transparent electrodes. Transparent conductive oxides (TCOs) are mostly *n*-type, highly doped semiconductors with a large bandgap (typically 3.0–3.6 eV), such as fluorine-doped SnO_2 (FTO), Sn-doped In_2O_3 (ITO), and Al-doped ZnO (AZO). The choice of the TCO is made on the basis of the solar cell process requirements, such as the layer deposition temperature and the chemical treatment, as well as the cell architecture. For example, CdTe-absorber cells have a superstrate architecture, where light enters the cell through the TCO-coated glass substrate. As TCO, SnO_2, or

ITO are predominantly employed, depending on the deposition temperature of the overlaying *n*-layer (CdS) and of the absorber. For lower deposition temperatures, ITO is the material of choice, because it presents better optical transmittance for a given sheet resistance. For higher temperatures, SnO_2 is favored for its greater stability. In CIGS cells, with a substrate architecture, the TCO is deposited last, after the absorber, forming the front contact. In this case, AZO is employed, as it has low cost and appropriate work function. Apart from the low resistive AZO, it is standard in CIGS cells that a so-called "window layer" is used, in the form of a highly resistive intrinsic ZnO. The role of the window layer is to reduce the shunt resistance of the solar cell and provide a better band alignment between the heterojunction and the TCO, increasing the open circuit voltage.

Similar to the ZnO buffer layer in CIGS cells, various metal oxides serve as interfacial layers for the anode and cathode, and they have been intensively researched for all types of thin film solar cells. Such interfacial layers improve the energy band alignment for hole and electron extraction, rendering the contact more selective to the specific carrier type [8,9]. Indeed, the work function of oxides spans a wide range from 3.5-7.0 eV. Low work function oxides, such as ZnO and TiO_2, are chemically stable and inert, in contrast to the low work function metals, such as Ca and Mg, which are very reactive. On the other hand, the high work function oxides, such as NiO or MoO_3 are low-cost materials compared to the high work function noble metals, such as Pt or Au. On top of that, certain oxides offer considerably larger work function values than what is possible with metals. Fig. 11.1 summarizes the energy band positions of some oxides, together with the work functions of metals that are used in solar cells.

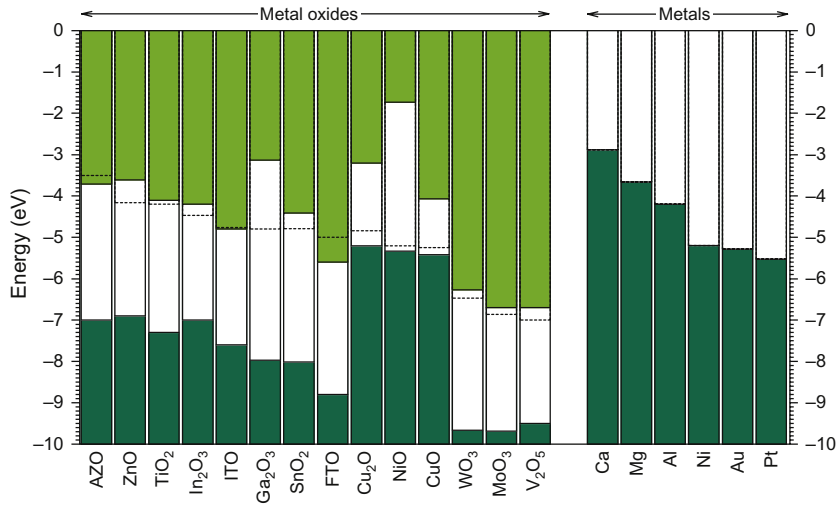

FIG. 11.1 Energy band positions of selected metal oxides that are relevant for photovoltaic cells, together with work functions of some metals used as anodes and cathodes. Presented data were compiled from the literature [8–20].

Last, nanostructured solar cells based on metal-organic sensitizers (dye-sensitized solar cells) [21] or organo-halide perovskite absorbers [22] rely on the use of 3D metal oxide scaffolds, in which the light absorbers are infiltrated, with the most common materials being a TiO_2 mesoporous layer and ZnO nanorods. These 3D components serve as electron transport layers, in contact with the solar cell cathode.

11.4 DRIVES FOR RESEARCH IN ALL-OXIDE SOLAR CELLS

Various metal oxide semiconductors offer abundance, nontoxicity, chemical stability, and high-throughput, low-cost manufacturing. Some of these oxides have also appropriate bandgap values to be used as active solar absorbers in PV cells. When combined with other metal oxides serving as buffer and TCO layers, all-oxide devices arise. However, the short lifetime of photo-excited carriers and the limited mobility of minority carriers compromise the functionality of metal oxide absorbers.

Probably the most promising metal oxide for use as an absorber is cuprous oxide (Cu_2O), with a bandgap of 2.1 eV, which we will discuss in detail later in the chapter. Bandgap values of this order are not ideal for single junction cells, but still they can deliver around 20% maximum efficiency under AM1.5 illumination [7]. Real-life efficiencies above 10% could still enable commercialization, if the total module cost were low and the long-term stability ensured.

Further, the relative high bandgap oxides are promising for use in more elaborate cell concepts. One of these concepts is the intermediate band solar cell. The main idea behind it is to highly dope the absorber with impurities that form an energy band partway inside the material's bandgap. This permits an electron to be excited across the bulk bandgap by absorbing two lower-energy photons: one exciting the electron from the valence band to the intermediate band, and the second, from the intermediate band to the conduction band. Otherwise wasted, low-energy photons can be thus used for carrier generation. Theoretical detailed balance calculations determine the ideal absorber bandgap for the case of intermediate band solar cells to be 1.9 eV, which value is very similar to the bandgap of Cu_2O. The calculated maximum power conversion efficiency for IBSC under maximally concentrated light is the impressive 63.2% [23].

Another application concept for higher bandgap absorbers is the tandem solar cell. In this case, two *p-n* junctions are stacked one upon the other, monolithically, into a two-terminal device. The junctions combine absorbers of different bandgap in order to absorb a larger spectrum of the solar irradiation. Cu_2O, with its high bandgap value, is targeted as the top junction absorber. Detailed balance thermodynamic calculations have shown that for a current-matched, double junction cell with Cu_2O as the top junction absorber, the ideal bottom

junction absorber would have a bandgap of 1.58 eV (within the range of various inorganic or perovskite absorbers), and that would lead to an overall efficiency of 34% [24].

11.5 Cu_2O-BASED SOLAR CELLS

Cuprous oxide (Cu_2O) is one of the first known semiconductors. Rectifying diodes based on this material where introduced as early as the mid-1920s, long before the emergence of silicon [25]. The photoelectric effect in Cu_2O was also identified very early [26], but at that time, the harvesting of light for energy generation was only a matter of scientific curiosity. Cu_2O was the material on which many fundamental theories of semiconductors were applied. Boris Davydov in 1938 explained the rectification properties of semiconductor junctions, introducing the notions of minority carriers and surface states [27,28]. Mott also applied his theory on rectification on the Cu/Cu_2O model device [29] and so did Schottky when discussing the notion of the potential barrier at a metal/semiconductor interface [30]. In the beginning of the 1950s, Si doping was achieved, and Si became the cornerstone of the semiconductor industry (including PV) with the introduction of the *p-n* homojunction [31]. In the 1950s and 1960s, the now-commercialized thin film PV technologies based on CdTe and CIGS absorbers started to develop. Until the 1970s, interest in a Cu_2O absorber remained very low, and technological advancements towards the development of a Cu_2O-based solar cell were sporadic and underwhelming.

The energy crisis in the 1970s brought renewed interest in low-cost PV, and Cu_2O enjoyed a few years of increased research attention, but that faded again with the end of the energy crisis. Cu_2O is once again attracting attention, driven (as before) by the need for abundant and environment-friendly PV materials, and aided by the technological advancements in thin film, heterojunction solar cell technology (which, when applied to Cu_2O cells enhance their energy conversion efficiency). In the study of Wadia et al., Cu_2O figures as one of the most intriguing candidates among inorganic absorber materials for supplying abundant and affordable electricity [4]. Cu_2O can be prepared by various vacuum and nonvacuum techniques, such as the thermal oxidation of Cu sheets [32–34], electrochemical deposition (ECD) [35], spray pyrolysis [36], anodic oxidation [37], chemical oxidation [38], SILAR [39,40], laser deposition [41], thermal evaporation [42], chemical vapor deposition (CVD), [43] and sputtering [44].

11.5.1 Material Properties

Cu_2O is composed of abundant and nontoxic elements. Its structure (cuprite) is cubic, with a lattice parameter of 4.27 Å. The Cu atoms are arranged in a fcc sublattice and the O atoms in a bcc sublattice (Fig. 11.2). Cu_2O belongs to the $Pn\bar{3}m$ space group. It has a spontaneous *p*-type conductivity due to a large concentration of negatively-charged Cu vacancies with low formation energy,

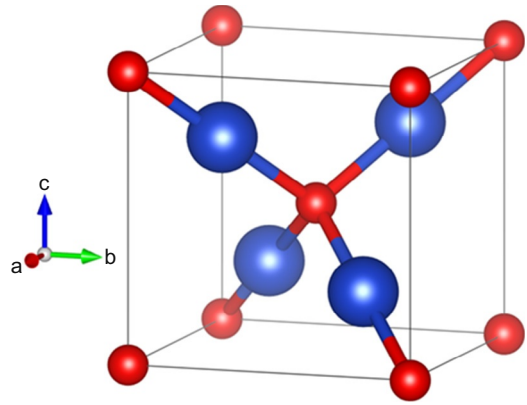

FIG. 11.2 Cubic structure of the Cu_2O crystal, with the O atoms (red spheres) arranged in a bcc sublattice and the Cu atoms (blue spheres) in an fcc sublattice. The space group is the $Pn\bar{3}m$. (Crystal structure produced using the VESTA software [45].)

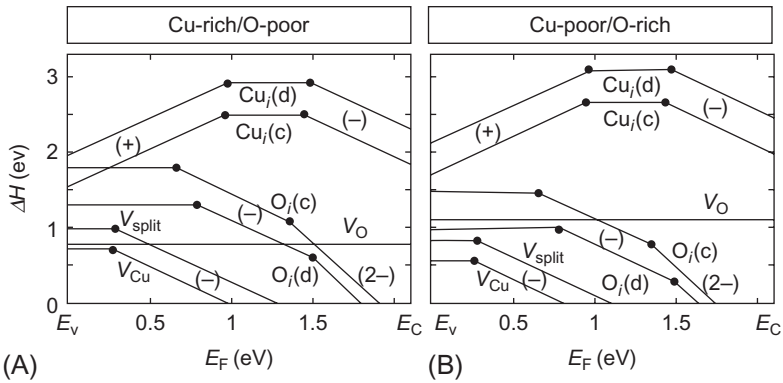

FIG. 11.3 Formation energies for intrinsic defects in Cu_2O in (A) Cu-rich/O-poor conditions and (B) Cu-poor/O-rich conditions. Only lowest energy charge states are shown; ionization levels are indicated with a dot. V_{Cu} and Cu_i denote copper vacancy and copper interstitial, respectively. V_O and O_i are oxygen vacancy and oxygen interstitital, respectively. V_{split} denotes a split vacancy, consisting of two Cu vacancies and a copper interstitial. "c" and "d" denote different interstitial site symmetries. *(Reprinted figure with permission from H. Raebiger, S. Lany, and A. Zunger, Phys. Rev. B. 76, 045209, 2007. Copyright 2007 by the American Physical Society.)*

which introduce a shallow acceptor level (about 0.2–0.3 eV above the valence band) and give rise to delocalized holes [46,47]. The Cu vacancy concentration is estimated in the order of 10^{18}–10^{20} cm^{-3}. The hole concentration, however, is orders of magnitude lower, as only a fraction of the vacancies will release a hole to the valence band at room temperature [46,48]. Ab initio calculations have shown that positively charged Cu interstitials, which could act as hole killers, have too-high formation energy to be significant under equilibrium growth conditions, while the low formation energy O vacancy is stable only in a charge-neutral state, which does not compensate hole doping (Fig. 11.3) [46].

Cu_2O has a direct bandgap of approximately 2.1 eV, but the optical transition at the bandgap energy is parity-forbidden [49], leading to a weak absorption onset. The top of the valence band is derived from Cu 3*d* states with a minor contribution from Cu 4*s* states. About 2 eV below, the O 2*p*-derived band is found. The lowest energy conduction band states are derived from a mixture of Cu 4*s* and Cu 3*d* states [46]. The highly dispersed and delocalized Cu 3*d* valence band gives rise to a low hole effective mass (0.4–0.5 m_e) and consequently large hole mobilities [50], which are experimentally determined above 100 cm^2/Vs for high quality films [33,34,51,52]. This is combined with a high absorption coefficient for energies above the bandgap of 10^3 up to more than 10^5 cm^{-1} [53]. The minority carrier diffusion length in Cu_2O depends on the film quality. In Cu_2O films fabricated by thermal oxidation, it can reach up to 12 μm [33,52]. On the contrary, in small crystal-size samples (100–200 nm), values as low as 430 nm have been reported [54].

A large number of reports exist concerning the introduction of doping into the Cu_2O, using a multitude of elements, such as: cadmium [32], nitrogen [55–58], chlorine [33,34,52], silicon [59], zinc [60], manganese [61], nickel [62,63], strontium [64], and sodium [65]. In all of these cases the conductivity remained *p*-type. Indeed, a changeover from *p*- to *n*-type by doping is not expected, due to the mechanism of self-compensation [66]. This means that, if we dope the *p*-type Cu_2O with donors, these are compensated by the creation of negatively-charged Cu vacancies. Tsur and Riess [66] quantitatively calculated that, depending on the dopant concentration and oxygen pressure, the hole concentration can decrease and the electron concentration increase at most by a factor of 10. Therefore one does not expect to obtain an *n*-type Cu_2O by doping, under equilibrium conditions.

The most frequently reported *p*-type dopant is nitrogen, which, with a preferred oxidation state of −3, is expected to act as an acceptor when substitutional incorporated into the oxygen lattice site. Indeed, Ishizuka et al. [55] have shown a roughly proportional dependence of the hole density on the nitrogen flow rate for rf magnetron sputtered Cu_2O films, varying from 10^{15} to 10^{17} cm^{-3}. The increase in hole density was accompanied by a 2- to 3-fold decrease in the hole mobility from its initial value of 30–60 cm^2/Vs, due to enhanced ionized acceptor scattering. The resistivity of the doped films decreased to a minimum of 15.2 Ω cm, while practically no effect of the doping on the bandgap was found. The nitrogen acceptor level was estimated at about 0.15 eV from the valence band [55]. In another work with similarly prepared Cu_2O films, the introduction of N rather generated O vacancies than acting as an acceptor. The resulting N-doped films had the same hole density as the un-doped one (10^{16} cm^{-3}) but the bandgap widened from 2.1 to 2.5 eV, as a consequence of the structural changes induced by the larger ionic radius of N (1.71), as compared to O (1.40) [56]. In Cu_2O films prepared by radical oxidation, treatment with N plasma induced both an increase of the hole density (simultaneously decreasing the mobility) and a blue shift of the bandgap from 1.69 to 2.42 eV [57]. A new aspect of N doping was underlined by Malerba et al. [58] who, apart from the

observed reduction in the resistivity and carrier mobility in rf-sputtered films, the authors found that N doping induces optical transitions between extended states and impurity discrete states, suggesting the application of this material for intermediate band solar cells [58].

Chlorine, with an oxidation state −1, should act as a donor in the case of substitutional incorporation in the oxygen site. Contrary to the expectation, Cl doping was shown to increase the hole density in Cu_2O. There can be two possible explanations for this, as suggested by Olsen et al. [33]. The first is that Cl is interstitially incorporated, leading to an acceptor level. The second is that Cl substitutes the oxygen, acting therefore as a donor, but the consequent rise of the Fermi energy leads to the formation of Cu vacancies, which increases the density of holes as a net effect. Musa et al. [34] made reference to the same reasons to explain the resistivity decrease in Cl-doped thermally oxidized Cu_2O films. Bicarri et al. [52] suggested that Cl can also substitute intrinsic oxygen vacancies, which are double donor defects, reducing therefore the minority carriers. In fact, the authors claimed that all three aforementioned mechanisms take place in Cl-doped thermally oxidized Cu_2O films, leading to a decrease of the resistivity and a reduction of photo-induced metastable effects as compared to un-doped films. Albeit, the authors claimed that the minority carrier lifetime is reduced in Cl-doped films, leading to a decrease of the power conversion efficiency in solar cells [52].

To briefly discuss cation dopants, Cd was shown to reduce dramatically the Cu_2O resistivity from 10^4-$10^5\,\Omega$cm down to $9\,\Omega$cm for approximately 1% Cd incorporation. Nevertheless, the mechanism of doping was not clarified [32]. Si was found to be an effective *p*-type dopant by forming silicate in Cu_2O [59]. Ni is an interesting case, since it was theoretically predicted to introduce a swallow acceptor level and enhance the *p*-type conduction [67]. The experimental results, nevertheless, suggested that Ni is incorporated interstitially as a neutral impurity, decreasing the mobility but not affecting the carrier density [62]. In the case of Sr incorporation, the observed effect of resistivity decrease could not be conclusively attributed to Sr doping or to induced morphological changes in the film [64].

Na doping has been proven the most efficient in controlling the hole concentration in thermally oxidized Cu_2O, without negative effects on the mobility. Minami et al. [68], obtained resistivity values in the range of 10^3–$10^{-2}\,\Omega$cm, associated with a hole concentration of 10^{13}–$10^{19}\,cm^{-3}$, while maintaining a Hall mobility above $100\,cm^2/Vs$ for hole concentrations below $10^{16}\,cm^{-3}$. It was suggested that the Na is incorporated at interstitial sites, acting as a donor and provoking the formation of Cu vacancies due to the charge compensation effect, giving rise to a net hole doping [68].

The above experimental and theoretical results show that it is extremely challenging to obtain *n*-type doping of the Cu_2O, as *n*-type defects have either very high formation energy, or they do not act as swallow donors, or further, they provoke the creation of acceptor defects due to charge compensation

effects. Despite this, a considerable amount of papers exist in the literature, reporting *n*-type conductivity in electrodeposited Cu_2O films [69–75]. Scanlon and Watson [76] have reviewed some of these reports and concluded that from the theoretical perspective, none of the alleged defects could lead to *n*-type doping and the presence of an inversion layer at the Cu_2O surface can be most probably held responsible for the apparent *n*-type conductivity, as proposed by Nian et al. [77].

11.5.2 Types and PV Performance of Cu_2O Solar Cells

11.5.2.1 Schottky Junction Cells

Cu_2O solar cell research in the 1970s and early 1980s concentrated on the Schottky junction architecture. The semiconducting absorber was fabricated by oxidizing high purity copper sheets at temperatures around 1000°C in order to obtain polycrystalline material, with grain size in the order of several hundred micrometers up to several millimeters, depending on the extent of the oxidation. A partially oxidized Cu sheet would result to the so-called "back-wall" Cu/Cu_2O junction that was used as the first rectifier device. For solar cells, the "front-wall" architecture was employed, where the thin Cu layer (~10 nm) was evaporated on the one side of the polished and cleaned wafer (>100 μm-thick), while at the other side an ohmic contact was formed [17,32,33,78]. By 1982, the work done on this type of cells resulted in a maximum power conversion efficiency, η, of 1.8%, with short circuit current, j_{sc}, of 8.5 mA/cm^2 and open circuit voltage, V_{oc}, of 0.36 V. In 1986, Iwanowski et al. [79] reported efficiency of 1.8% on front-wall Cu_2O/Cu solar cells that have been H+ ion-bombarded after the vacuum deposition of the thin Cu layer. $V_{oc} = 0.525$ V and $j_{sc} = 7.35$ mA/cm^2 were achieved. It was suggested that the improvement of the quality of the reduced Cu_2O/Cu interfacial layer was the reason for this improvement.

Attempts were made to replace Cu with a range of low-work function metals, such as Mg, Yb, and Mn in order to increase the Schottky barrier height and, by that, the V_{oc}. Unfortunately, the replacement of the metal had almost no influence on the junction properties. The reason was the uncontrollable reduction of Cu_2O at the interface with the metal, giving rise to a Cu-rich region, which essentially determined the barrier height [17]. Free energy calculations have shown that the use of Thallium (Tl), another low work-function (3.7 eV) metal, should prevent Cu_2O reduction. In praxis, however, also Tl proved unsuccessful to increase the barrier height that remained in the range of 0.7–1.0 eV. The suggested reason was a preferential sputtering of the oxygen from the absorber surface during the metal deposition, leading to a Cu-rich interface [33]. In the same work it was found that Au forms a very low barrier height (practically ohmic) contact with Cu_2O.

The conclusion drawn from these investigations was that the Schottky solar cell architecture was unable to deliver high conversion efficiencies. Taking into account the challenge of achieving *n*-type Cu_2O, it was proposed to focus on

the metal-insulator-semiconductor (MIS) structure, where the insulator inhibits interfacial reduction and blocks majority carrier flow. Alternatively, one could form an *p-n* heterojunction with a material that does not react with Cu_2O [17].

11.5.2.2 Heterojunction and MIS Solar Cells

As early as 1981, Papadimitriou et al. [80] reported heterojunction solar cells on thermally oxidized Cu_2O with sputtered In_2O_3, SnO_2, CdO, mixture of SnO_2-CdO and thermally evaporated ZnSe. Similar to the Schottky cells, chemical analysis of the interface showed in all cases, except for the CdO, evidence of metal Cu, arising from chemical reactions. Consequently, the PV performance was very poor. Only Cu_2O/CdO cells showed $V_{oc}=0.4\,V$, but small current of $2\,mA/cm^2$. Practically the same effect of Cu-enriched interface was observed for heterojunctions with rf-sputtered In-doped ZnO, resulting in cells of poor performance and V_{oc} in the order of 0.3 V [81].

In 2006, 24 years after the highest reported efficiency of 1.8% [33], Mittiga et al. [51] achieved 2% efficiency for an heterojunction cell on a Cu_2O substrate (see Fig. 11.4A), prepared by a two-step thermal oxidation in N_2/O_2 atmosphere

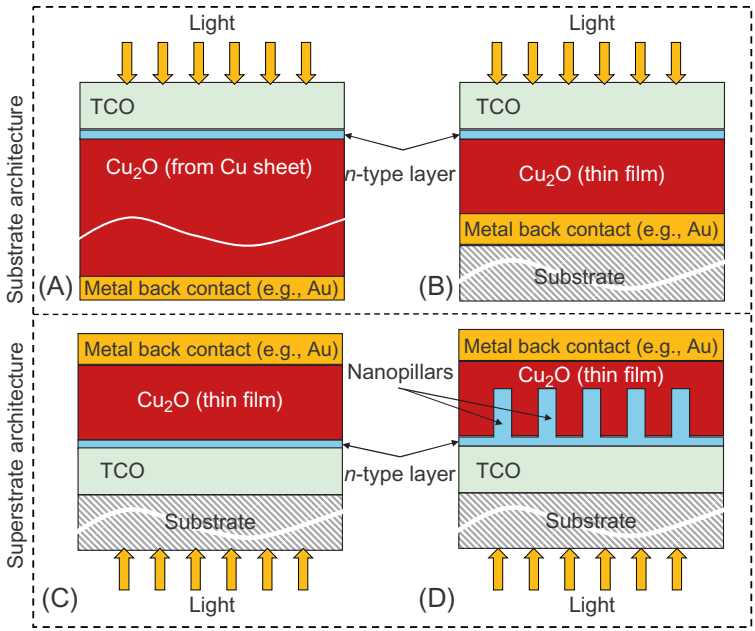

FIG. 11.4 Types of Cu_2O absorber cells. (A) Substrate cell architecture where a Cu sheet (typically 100–250 μm-thick) is thermally oxidized to form the Cu_2O absorber. The rest of the cell components are deposited by vacuum techniques. (B) Substrate cell architecture, where a Cu_2O thin film is deposited by vaccum or solution-based techniques onto a metallic back contact. (C) Superstrate architecture, where the Cu_2O thin film absorber is deposited on the transparent contact. (D) Another substrate architecture, in which the transparent contact is nanostructured (e.g., nanopillars) and the Cu_2O thin film absorber fills the voids of the structured contact.

and maximal processing temperature >1100°C. This substrate preparation allowed to obtain grains in the order of 1 mm^2, with low defect density and carrier mobility in the order of 100 cm^2/Vs. On the cleaned and etched Cu_2O substrate (to remove the CuO surface layer), ITO or ZnO/ITO were deposited by ion beam sputtering at room temperature, followed by a Cu grid to facilitate current extraction, a MgF_2 antireflection coating to reduce optical losses and the evaporation of an Au layer at the back side of the substrate as ohmic contact. Cu_2O/ZnO/ITO cells achieved efficiency of 2%, $V_{oc} = 0.6$ V and $j_{sc} = 6.8$ mA/cm^2. Cu_2O/ITO cells did not perform as well, which was attributed to the higher electron affinity of ITO as compared to ZnO, lowering the built-in potential of the junction. It should be noted, however, that the ITO and ZnO layers had reported resistivity values of 10^{-3} and 3×10^{-3} Ω cm, respectively. They could be therefore considered as degenerate semiconductors and their contact to the Cu_2O absorber as a Schottky type. Similarly to the previous work, a highly doped Ga:ZnO film, produced by vacuum arc plasma evaporation (VAPE), was used to form a junction to Cu_2O, which functioned more as a Schottky barrier and achieved conversion efficiency of 1.52% [82]. This work also concluded that, to obtain high quality junction, a deposition method for the *n*-type layer should be chosen that does not cause strong oxidation of the Cu_2O surface and does not utilize high density and high energy plasma. To this end, pulsed laser deposition or VAPE have a competitive advantage over magnetron sputtering [82].

The advantage of using PLD, as a low-damage technique, to fabricate the *n*-type layer was exploited several times during the following years by the group of Minami. In 2011, 3.83% efficiency, with $V_{oc} = 0.69$ V and $j_{sc} = 10.1$ mA/cm^2 were achieved for a Cu_2O/ZnO/AZO *p-n* junction, with room temperature PLD-grown ZnO/AZO [83]. These values were later moderately improved to 4.12%, 0.72 V and c.10 mA/cm^2, respectively [84]. Despite the remarkable improvement in efficiency, fact is that the Cu_2O/ZnO heterojunction features a large conduction band misalignment of approximately 0.9 eV [85], giving rise to enhanced carrier recombination losses and reduced V_{oc}. So, other more appropriate alternatives for the *n*-type layer were investigated, with the aim to reduce its electron affinity.

It was observed that the alloying of ZnO with Mg widens the bandgap of the $Zn_{1-x}Mg_xO$ layers and shifts the conduction band minimum closer to the vacuum level, so that a better band alignment can be achieved with the low electron affinity Cu_2O layer. The widening of the bandgap with increasing Mg content, *x,* can be quite large (3.2–3.9 eV) and follows a practically linear relation for *x* up to c.0.30, where the wurtzite phase is also maintained. For larger Mg contents up to ~0.45, a mixed wurtzite-cubic phase material is obtained without further bandgap increase, while for $x > 0.45$ the cubic phase prevails [86]. The linear dependence of the bandgap on *x* has been observed for films prepared by a variety of techniques (sputtering, PLD, etc.) [86–89] Motivated by this feature, $Zn_{1-x}Mg_xO$ films were grown by PLD on the thermally oxidized Cu_2O substrates, leading to an increase of the V_{oc} for $x < 0.18$, compared to the ZnO reference, from 0.71 V to more than 0.8 V. The maximum efficiency of 4.31% was obtained in a $Cu_2O/Zn_{0.91}Mg_{0.09}O$/AZO

heterojunction solar cell. Further increase of the Mg content led to a drastic decrease of the efficiency due to the degradation of the solar cell's j_{sc} and fill factor (FF). This degradation was attributed by the authors to the increase of the $Zn_{1-x}Mg_xO$ layer resistivity for increased Mg content [90].

The next step of the Minami group was to investigate *n*-type Ga_2O_3, motivated by its lower electron affinity compared to ZnO [15,91]. The employment of a PLD Ga_2O_3, grown at RT, to form the heterojunction, increased the V_{oc}, relative to the ZnO layer, from 0.71 to 0.8 V, but also the j_{sc} and the FF, attaining maximum efficiency of 5.38% [92]. The magnitude of the V_{oc} increase was, nevertheless, much lower than what expected from the assumed difference in the electron affinities between Ga_2O_3 and ZnO. On the contrary, it was found to correlate to the diffusion potentials yielded from capacitance-voltage measurements for the Cu_2O/ZnO and Cu_2O/Ga_2O_3 heterojunctions. Also, the very low leakage currents obtained for the Cu_2O/Ga_2O_3 cell suggested a reduction of the defect density at the heterojunction interface. In parallel, the external quantum efficiency in the window below 500 nm was increased for the Cu_2O/Ga_2O_3 cell, which was attributed to the enhancement of the lifetime of photo-excited electrons near the heterojunction. This was also attributed to the decrease in the defect levels.

A further improvement of the state-of-the-art was achieved from the same group, through a combination of Cu_2O substrate optimization and the implementation of PLD, *n*-type, amorphous aluminum gallium oxide ($Al_{1-x}Ga_x$-O) layers, with varying Al content [65]. Cells of $Cu_2O/Al_{0.025}Ga_{0.975}O$ outperformed the ones of Cu_2O/Ga_2O_3, obtaining 5.38% and 5.06% efficiency, respectively. After appropriate doping of the Cu_2O substrate with Na, following a heat-treatment in Ar gas atmosphere for 1 h to impregnate NaI, the resistivity of the substrate could be reduced from 10^3 to $10^{-1}\,\Omega$cm [68]. The drastic doping effect of the Na was explained by the production of Cu vacancies that result from charge compensation effects when a Na atom is incorporated at an interstitial site in the Cu_2O lattice and acting as a donor. Most importantly, it was also found that the incorporation of Na into the Cu_2O absorber was homogenous throughout its thickness and that the levels of Na dopant corresponded to the levels of hole concentrations, suggesting a high degree of dopant activation [65]. The doping did not influence the carrier mobility, which remained in the range of 100 cm^2/Vs. Finally, the employment of a Na:Cu_2O substrate (with resistivity of 15 Ω cm) together with an optimized $Al_{0.025}Ga_{0.975}O$/AZO n-layer and an MgF_2 antireflection coating, gave rise to an efficiency of 6.1%, $V_{oc} = 0.84$ V, $j_{sc} = 10.95$ mA/cm^2 and FF = 66%. This result is therefore the combined effect of reducing ohmic losses in the absorber, as well as lowering the defect density and improving the band alignment at the heterojunction.

The course of development of Cu_2O heterojunctions with PLD *n*-layers led to the mixed ZnO-GeO_2 composite ternary compound. The band structure parameters of these compounds, such as the work function and bandgap, have been shown to be controlled by the composition of their component oxides [14]. The motivation for investigating this oxide combination was again to decrease

the electron affinity of ZnO by mixing it with the lower electron affinity GeO_2 (c.2.5 eV) [93–95]. Solar cells employing the amorphous *n*-type semiconductor zinc germinate (Zn_2GeO_4), fabricated by PLD, in the device Cu_2O/Zn_2GeO_4/AZO, have shown very low efficiency of 0.03% [96]. The same group continued the research on this material, investigating a range of compositions, thicknesses and growth conditions, in order to improve the efficiency. Their work is reported in a recent paper [97]. This time, the best produced solar cells of Cu_2O:Na/$Zn_{0.38}Ge_{0.62}$-O/AZO/MgF_2 yielded efficiency of 8.1%, with $j_{sc} = 11\,mA/cm^2$ and $V_{oc} = 1.16\,V$, which are all-time record values for Cu_2O solar cells.

An atypical MIS-type of solar cell on thermally oxidized Cu_2O was reported by Ergen et al. [98]. In their approach, a 25 μm-thick Cu foil was used to grow a thin layer (~15 nm) of hexagonal boron nitride (*h*-BN) by chemical vapor deposition on both sides of the foil. The layer was removed from the bottom side of the foil, while it remained on the top. With the thermal oxidation of the foil, the side covered with the *h*-BN was protected against formation of CuO. For optimized devices, at the bottom side, the CuO was left intact and a Cr/Au ohmic contact was deposited. From the top side now, the *h*-BN layer was thinned, by using a scotch-tape technique, to a thickness of 1–6 nm, before evaporating a 5 nm-thick Cu top contact. Devices with this architecture deliver efficiency of 3.44% with $V_{oc} = 0.52\,V$ and $j_{sc} \approx 10\,mA/cm2$, while only 2% efficiency was obtained for Schottky cells without the *h*-BN layer.

The PV performance of thermally oxidized Cu_2O-substrate solar cells has seen an enormous improvement in the last 10 years, with the efficiency rising from 2% to more than 8%. However, the demand remains to obtain efficient solar cells with thin film absorbers, having low material consumption and low fabrication cost. To this end, the electrochemical deposition (ECD) of Cu_2O has a large potential, as it takes place close to room temperature (around 50–60°C) and from solutions of low-cost chemical reagents, such as copper sulfate, lactic acid and sodium hydroxide [35]. Electrochemical deposition of films offers precise control of the driving force for the reactions involved in deposition, allowing control of the structure and phase composition of the films [35]. In addition, ECD is easily up-scalable, high throughput and compatible with roll-to-roll processing.

The investigations on ECD-Cu_2O solar cells are currently pursued with increasing intensity. Both potentiostatic (constant deposition potential) [99–105] and galvanostatic [54,106–110] (constant deposition current) methods have been reported. In Fig. 11.5, SEM images from a cell with potentiostatically grown Cu_2O are shown. The cell architecture is of the superstrate type (Fig. 11.4C), where the absorber is deposited on top of the *n*-layer. This prevents the contamination of the absorber's surface through exposure in air or other process gasses. The maximum achieved efficiency of solar cells with thin film, ECD-grown Cu_2O, remained for long time limited at 1.28% [107]. In this record-cell the Cu2O was deposited on a electrodeposited ZnO *n*-layer, residing on an FTO-coated glass.

Only recently could the efficiency of ECD-Cu_2O cells be considerably increased to 2.65% by employing an amorphous Sn-doped ZnO layer (ZTO) to

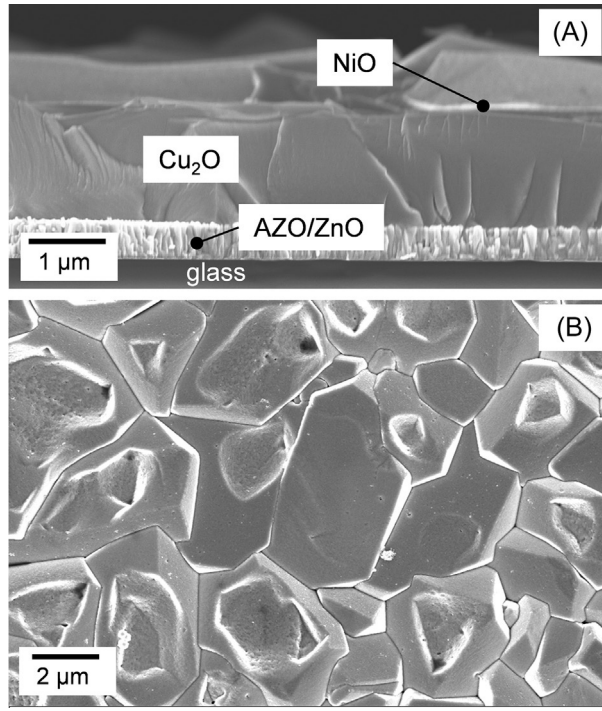

FIG. 11.5 Cross section and plane view SEM images of a superstrate-type cell with sputtered AZO/ZnO on glass, followed by the Cu_2O absorber, electrochemically deposited in potentiostatic mode. After the absorber, a thin interfacial layer of NiO is deposited before the deposition of the Au top contact (not shown). The cell yielded an efficiency of 1.12%. *(Adapted from T. Dimopoulos, A. Peić, S. Abermann, M. Postl, E.J.W. List-Kratochvil, R. Resel, Effect of thermal annealing in vacuum on the photovoltaic properties of electrodeposited Cu2O-absorber solar cell, EPJ Photovolt. 5 (2014) 50301. doi:10.1051/epjpv/2014005.)*

form the heterojunction, using atomic layer deposition (ALD) and a substrate-type of solar cell architecture [110], with Ag or Au as bottom electrode. ALD is a low-damage deposition process that covers rough surfaces in a conformal and uniform manner. To this respect, it is a suitable method for the formation of high quality, defect-poor interfaces. In the used substrate-type of cell (Fig. 11.4B), the surface of the Cu_2O absorber is exposed to air and, as a result, a thin CuO layer is formed. It was found that this layer can be reduced to Cu_2O, in the first stages of the ALD process, by the reactive diethylzinc (DEZ) precursor used for the deposition of the ZnO. This reduction allowed to attain the aforementioned high cell efficiency. By decreasing the deposition temperature of the *n*-type layer from 120°C to 70°C, the defects at the heterojunction interface were reduced and the efficiency further increased to 3.06% [111].

Finally, Lee at al. reported the highest efficiency for ECD-Cu_2O cells of 3.97%, through the implementation of an ALD Ga_2O_3 layer with the thickness

of 10 nm [112]. An impressive open circuit voltage of 1.2 V was reached, being mainly the result of an optimized band alignment at the heterojunction. Indeed, the energy band alignment at the Cu_2O/Ga_2O_3 interface was investigated by X-ray photoelectron spectroscopy and the conduction band offset was determined to be 0.18 eV (cliff), with a valence band offset of 3.27 eV, indicating a type-II heterojunction. Most importantly, the deposition of the Ga_2O_3 reduced the CuO layer on the absorber's surface to Cu_2O. This breakthrough result for this type of cells is the outcome of both choosing a layer with an appropriately low electron affinity and reducing interfacial defects. Further improvement of the PV performance could be achieved if the carrier collection length could be enhanced and the series resistance of the solar cell decreased. If these issues are addressed, the authors estimated the j_{sc} to increase from the present 7.37 to 11.5 mA/cm^2 and the FF from 44.7% to 84%, giving rise to a device efficiency approaching 11.5% [112].

Besides Ga_2O_3, the band offset values of PLD $Zn_{1-x}Mg_xO$ with $x=0.06$ and 0.21 to ECD-Cu_2O were investigated by Brandt et al. [113]. A staggered, type II heterojunction was found with conduction band discontinuities of 1.15 and 0.97 eV respectively. Similar band alignment results were reported with ALD $Zn_{1-x}Mg_xO$ for a wide range of compositions ($0 \leq x \leq 0.22$). The maximum achieved efficiency in the last case was 1.67% with $V_{oc}=0.55$ V for $x \approx 0.10$ [114]. Last, $Zn_{1-x}Mg_xO$ ($0 \leq x \leq 0.13$) films grown by metal-organic chemical vapor deposition (MOCVD) on electrodeposited Cu_2O [115] led to an efficiency of 0.71% (for $x=0.10$). From these results, it can be concluded that, although the alloying of ZnO with Mg decreases its electron affinity, the misalignment with the conduction band of Cu_2O remains exceedingly large to achieve high V_{oc} values.

Apart from the $Zn_{1-x}Mg_xO$, the band offsets of a number of *n*-type, electron-selective contacts on Cu_2O, have been investigated by XPS [113]. The results revealed two main strategies on the development of such layers: the first relies on creating ternary compounds, by alloying on the anion site with larger isovalent elements, so as to push the conduction and the valence band to higher energies. The authors identified Zn(O,S) with sulfur content >70%, as an ideal material to match the conduction band position of Cu_2O and suggested that also intermediate compositions of (Zn,Cd)S would lead to favorable alignment. The second strategy involves the use of low electron affinity materials, such as Ga_2O_3, with the need to increase their carrier concentration, in order to reduce the device series resistance and further increase the device performance.

Besides ECD, other techniques have been employed for the fabrication of thin film Cu_2O in solar cells. Recently, SILAR (successive ion layer adsorption and reaction) was used for the Cu_2O deposition, in solar cells with the architecture glass/ITO/NiO/Cu_2O/ZnO/SnO_2/Al [40]. All other oxides, apart from the ITO-coated glass, were deposited from nanoparticle solutions. The solar cells yielded $\eta=1.12\%$, $V_{oc}=0.64$ V and $j_{sc}=3.50$ mA/cm^2. In another interesting case, PLD was applied to form heteroepitaxial thin film Cu_2O (~0.5 μm) solar cells on buffered, low-cost, flexible NiW foils. By optimizing oxygen pressure and temperature of deposition, Cu_2O films with mobilities in the range of

50–60 cm^2/Vs could be achieved and carrier densities in the order of 10^{16} cm^{-3}. By implementing *n*-type ZnO layer to form the heterojunction, an efficiency of 1.65% was obtained, with $V_{oc}=0.65$ V and $j_{sc}=5.7$ mA/cm^2 [116].

11.5.2.3 Nanostructured heterojunction cells

Heterojunction solar cells include cells that use a nanostructured, *n*-type electrode, on top of which the Cu_2O absorber is deposited. The absorber fills the voids of the electrode, creating a folded heterojunction (Fig. 11.4D). The Cu_2O is, in the majority of cases, deposited by electrodeposition, but there are reports where sputtered or nanoparticle-based absorbers have been used. For what concerns the nanostructured electrode, ZnO nanorods (NRs) are predominantly employed, grown on a TCO film via a solution-based technique, like ECD or hydrothermal method [100,103,109,117–123]. Besides, ZnO nanotubes (NTs) [122], fibrous networks [124], and anodized TiO_2-NT membranes have been reported [125].

The purpose of a nanostructured electrode is twofold. Firstly, it amplifies the active junction area of the solar cell, which should lead to an enhancement of the extracted current. Secondly, it decouples the light absorption and carrier extraction to orthogonal directions, reconciling short carrier transport distances with thick absorbing layers. This type of solar cell design is therefore particularly interesting for absorbers with low minority carrier diffusion lengths.

Up to now, Cu_2O nanostructured solar cells have not lived up to the expectations of PV performance enhancement. The best result was reported by Cui et al. [100] on glass/ITO/ZnO/ZnO-NRs/Cu_2O/Au solar cells, where the NRs and the absorber were electrodeposited (Fig. 11.6). The efficiency was 0.88%, with $j_{sc}=8$ mA/cm^2 and $V_{oc}=0.29$ V. For comparison, the planar solar cell (without nanorods) yielded efficiency of 0.55%, $j_{sc}=4.3$ mA/cm^2 and $V_{oc}=0.33$ V. A significant increase of the collected current in the nanostructured cell could be therefore achieved with a small decrease in the voltage. This behavior cannot be generalized. For instance, in a similar work from Musselman et al. [119], the efficiency of planar cells was more than double the one of the nanostructured, despite a small gain in the collected current. The degradation of the nanostructured cell's efficiency was driven by the large reduction of the V_{oc} from 0.41 V (for the planar cell) to only 0.23 V and a decrease of the FF from 48% to 34%. A promising result was recently obtained by Ebd-Ellah et al. [122], who achieved V_{oc} values of 0.66 and 0.71 V in electrodeposited ZnO-NT/Cu_2O and ZnO-NRs/Cu_2O cells, respectively. These are the largest V_{oc} values obtained for a nanostructured Cu_2O cell and similar to the best values obtained for highest-quality, planar ZnO/Cu_2O junctions. Unfortunately, at the same time the current was very small (in the best case 2.4 mA/cm^2), which reduced the overall efficiency to below 1%. The annealing of the cell structure is believed to have played a critical role on achieving these high V_{oc} values, by improving the crystallinity of the absorber, increasing the charge carrier concentration, from 4×10^{13} to 8×10^{13} cm^{-3}, and decreasing the heterojunction defect density [122].

The low carrier density in electrodeposited Cu_2O has been proposed as the main reason why, in most of the nanostructured cells, the achieved V_{oc} is smaller than in planar cells [119]. Due to the low carrier density, the depletion width in the planar

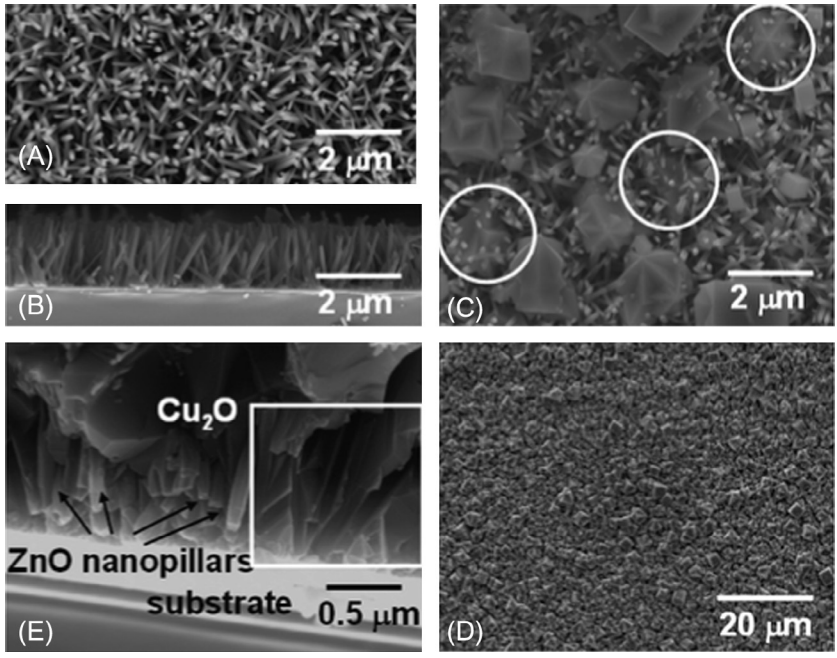

FIG. 11.6 SEM images of a nanostructured solar cell based on ZnO nanopillars (A and B), on top of which the Cu_2O absorber is electrodeposited (C and D), filling the voids of the nanopillars structure (E). *(Reprinted with permission from J. Cui, U.J. Gibson, J. Phys. Chem. C. 114 (2010) 6408. Copyright 2010 American Chemical Society.)*

cells extends over micrometer-range in the absorber layer [105]. In nanostructured solar cells, the voids between the nanopillars, which are filled by the absorber, are only a few hundred nanometers wide. This distance is insufficient to accommodate the full extent of the depletion region and, as a result, it does not enable the full built-in bias. Therefore, it was suggested [119] that the increase of the charge density in electrodeposited Cu_2O by doping is of critical importance in order to increase the V_{oc}.

11.5.2.4 Homojunction Cells

As we mentioned before, the *n*-type doping of Cu_2O is a challenging and rather controversial issue in the literature. Limited reports exist concerning Cu_2O homojunction solar cells, all of them fabricated by electrochemical deposition [74,126–130]. The best achieved efficiency was 1.06%, with $V_{oc}=0.61$ V and $j_{sc}=4.07$ mA/cm^2 [128]. In this work, the *p*-type part of the homojunction was electrodeposited on ITO-coated glass from a basic solution (pH ≈ 11) of copper sulfate, lactic acid, H_2SO_4 and NaOH, while the *n*-type from acidic solution (pH ≈ 4.9) of copper acetate, acetic acid and NaOH. ITO was used as a front contact. Most related papers in the literature use the aforementioned ECD recipe with small variations.

In Table 11.1, we summarize the most important solar cell performance results from the aforementioned categories.

TABLE 11.1 Summary of PV Performance Results From Best-Performing Cells, With the Cu_2O Absorber Fabricated by Thermal Oxidation of Cu Sheets, Electrodeposition or SILAR (HET Stands for Heterojunction, HOM for Homojunction)

Solar Cell Structure	Junction Formation	η (%)	V_{oc} (V)	j_{sc} (mA/cm^2)	Reference
Thermal oxidation of Cu_2O					
Au/Cu_2O/Cu(10 nm)/SiO_2 ARC (Schottky)	Evaporation of Cu	1.8	0.360	8.50	1982, Olsen et al. [33]
Au/Cu_2O/Cu (6 nm)/SiO_2 ARC, H^+ ion bombarded junction (Schottky)	Resistive evaporation of Cu	1.8	0.525	7.35	1986, Iwanowski et al. [79]
Au/Cu_2O/ZnO/ITO/Cu-grid/MgF_2 ARC (HET)	IBS of ZnO/ITO	2.0	0.595	6.78	2006, Mittiga et al. [51]
Au or Cu_2S/Cu_2O/ZnO/AZO (HET)	PLD of ZnO/AZO	3.83	0.690	10.09	2011, Minami et al. [83]
Au or Cu_2S/Cu_2O/$Zn_{0.91}Mg_{0.09}O$/AZO (HET)	PLD of ZnMgO/AZO	4.31	0.800	9.00	2012, Minami et al. [131]
Au/Cu_2O/Ga_2O_3/AZO (HET)	PLD of Ga_2O_3/AZO	5.38	0.800	9.99	2013, Minami et al. [92]
Au/Cu_2O:Na/$Al_{0.025}Ga_{0.975}O$/AZO/MgF_2 (HET)	PLD of $Al_{0.025}Ga_{0.975}O$/AZO	6.10	0.840	10.95	2015, Minami et al. [65]
Au/CuO:Na/$Zn_{0.38}Ge_{0.62}$-O/AZO/MgF_2 (HET)	PLD of $Zn_{0.38}Ge_{0.62}$-O/AZO	8.10	1.100	11.00	2016, Minami et al. [97]

Cr/Au/CuO/Cu_2O/***h***-BN/Cu (MIS)	CVD of h-BN Evaporation of Cu	3.44	0.520	10.50	2015, Ergen et al. [98]
ITO/$Zn_{0.79}Mg_{0.21}O$/Cu_2O/Au (HET)	Atmospheric ALD	2.2	0.650	6.90	2015, Ievskaya et al. [132]
Electrochemical deposition of Cu_2O					
Glass/FTO/ZnO/Cu_2O/Au (HET)	ECD ZnO	1.28	0.590	3.80	2007, Izaki et al. [107]
Glass/Ti/Au/Cu_2O/a-ZTO/AZO/Al grid (HET)	ALD a-ZTO/AZO	2.65	0.533	7.37	2013, Lee et al. [110]
Glass/Ti/Au/Cu_2O/a-ZTO/AZO/Al grid (HET)	ALD a-ZTO/AZO (with lower deposition temperature)	2.85	0.622	7.25	2014, Lee et al. [111]
Glass/Ti/Au/Cu_2O/Ga_2O_3/AZO/Al grid (HET)	ALD of Ga_2O_3	3.97	1.204	7.37	2014, Lee et al. [112]
Glass/ITO/ZnO/ZnO-NPs/Cu_2O/Au (nanostructured HET)	ECD of ZnO/ZnO-NPs	0.88	0.290	8.00	2010, Cui and Gibson [100]
Glass/ITO/***p***-Cu_2O/***n***-Cu_2O/ITO (HOM)	ECD of Cu_2O in acidic solution	1.06	0.610	4.07	2012, McShane and Choi [128]
SILAR of Cu_2O					
ITO/NiO/Cu_2O/ZnO/SnO_2/Al (HET)	Nanoparticle film	1.12	0.640	3.50	2016, Chaterjee et al. [40]

11.6 OTHER OXIDE-ABSORBER SOLAR CELLS

Apart from the Cu_2O absorber that dominates the research and literature in the topic of oxide solar cells, a multitude of other metal oxides exists with appropriate semiconductor properties for use as solar absorbers. In the following paragraphs, we will review materials investigated in the literature, namely CuO, Bi_2O_3, Pb_xO_y, Co_3O_4, and Fe_2O_3, for what concerns their basic material properties and their performance in photovoltaic cells.

11.6.1 CuO (Cupric Oxide) Absorber

Cupric oxide (CuO) and Cu_2O are the most common phases of copper oxides, with another uncommon phase, the paramelaconite (Cu_4O_3) with mixed Cu^{II} and Cu^{I} oxidation states [49]. CuO has been broadly investigated for practical applications (e.g., as the basis of high temperature superconductors, magnetic storage, gas sensing, photoelectrochemical catalysis, and photovoltaics). Its crystal structure (tenorite) is monoclinic with C2/c symmetry and four formula units per unit cell [133]. Like Cu_2O, CuO is also an intrinsic *p*-type semiconductor, owing to spontaneously formed and stable Cu vacancies [134]. The reported bandgap values broadly vary between 1.2 and 1.8 eV, and there is controversy in the literature about whether the bandgap is direct or indirect [16,75,135–139]. The majority of experimental data suggest an indirect type, which is also supported by band structure calculations [134,140,141]. From the analysis of the wave functions of CuO, the top valence band and the two bottom conduction bands have been attributed to the 3*d* orbitals of Cu atoms [134]. The calculated effective mass for holes along the DΓ direction is $0.78m_0$ and $3.52m_o$ along the transversal direction (where m_o is the electron rest mass). This yields an average effective mass of $1.87m_o$, which is much larger than the one of silicon [134]. Indeed, the *d* electrons are more localized than the *sp* electrons of silicon, giving rise to much smaller carrier mobilities.

As mentioned before, due to its lower bandgap than Cu_2O and the high absorption coefficient, CuO is attractive for solar cell application. Though, conversion efficiencies of CuO solar cells are still below the 1% threshold. In 2011, an efficiency of nearly 0.1%, $V_{oc}=0.37$ V and $j_{sc}=0.63$ mA/cm^2, were reported for CuO nanowires, grown from a Cu foil with thermal oxidation and covered with solution-processed *n*-type ZnO [142]. Dimopoulos et al. [137] fabricated glass/AZO/ZnO/CuO/NiO/Au sputtered heterojunctions and found maximum power conversion efficiency of 0.08%, obtained for a CuO thickness of 500 nm, for which also maximum $j_{sc}\approx 1$ mA/cm^2 was obtained. The V_{oc} was found to decrease from 400 to 250 mV as the CuO thickness increased from 400 to 900 nm. These results suggested that bulk recombination plays a major role in the photovoltaic performance. Morash et al. [139] prepared solar cell structures with FTO/TiO_2 front contacts and Au back contacts. The CuO had a thickness of nearly 70 nm.

Illuminated cells showed V_{oc} below 150 mV and photocurrent densities below 0.1 mA/cm^2. The authors attributed the poor values to the high defect concentration in CuO and the interface recombination at the TiO_2/CuO interface due to the staggered-type band alignment with a high conduction band offset. It was also reported that the deposition of Au onto CuO leads to a chemical reduction of the CuO surface.

Finally, the largest efficiency in CuO-based solar cells was reported using ZnMgO as *n*-type layer and PLD to form the heterojunction [143], with the complete structure being glass/ITO/CuO/ZnMgO/Ag. The highest efficiency of 0.253% was obtained for a Mg atomic content of 10%, with j_{sc} = 2.13 mA/cm^2 and V_{oc} = 0.326 V. The improvement was attributed to the reduction of the conduction band offset between CuO and ZnO with the addition of Mg doping, as it was also observed for the Cu_2O solar cells.

11.6.2 Bi_2O_3 Absorber

Bi_2O_3 combines interesting optical and electronic properties, such as energy bandgap values from 1.7 to 3.96 eV, high refractive index and dielectric permittivity, large ionic conductivity and photoluminescence [144]. These properties make the material attractive for optoelectronics, optical coatings, fuel cells, and gas sensors. Six polymorphs of Bi_2O_3 exist, labeled as: α-, β-, γ-, δ-, ε-, and ω-phases [145,146]. At room temperature, the stable phase is the monoclinic α-Bi_2O_3. Upon heating, the α-phase is transformed into the face-centered cubic δ-form, which is stable between 730°C and 825°C (the melting temperature of the material) [147]. The other faces are metastable, namely the tetragonal β phase near 650°C and the body-centered cubic γ phase at about 640°C, depending on the sample thermal treatment. Additional metastable forms are the orthorhombic ε polymorph and the triclinic ω-Bi_2O_3, which have been also reported in the literature.

Every polymorph has distinctive optical and electrical properties. With respect to the Bi_2O_3 band structure, Bi 6*s* and Bi 2*p* states contribute to the formation of the valence and the conduction band, respectively [148]. At the same time, the hybridization between Bi 6*s* states and O-2*p* ones, make the top of the valence band more dispersive, which enhances the hole mobility [148].

Although the δ phase is stable only at high temperatures, Fan et al. have reported δ-Bi_2O_3 thin films stable at room temperature, prepared by rf reactive sputtering in Ar/O_2 atmosphere [147]. They extracted an indirect bandgap in the range of 1.73–1.95 eV, depending on the amount of oxygen present during sputtering. Li et al. calculated the band structure of the α and β phase using the DFT GGA + U method and reported bandgap values of 2.803 and 2.436 eV, respectively, with both being of indirect type [148]. Gobrecht et al. [149], located the direct optical transition of α-Bi_2O_3 at 2.91 eV and the indirect

transition at 2.6 eV. These bandgap values, agree with the experimentally obtained 2.40–2.80 eV for a mixed system of α-Bi_2O_3 and β-Bi_2O_3, despite the fact that the authors obtained these values from Tauc plots assuming a direct band gap transition [150]. α-Phase Bi_2O_3 prepared by chemical bath deposition also presented a direct bandgap of 2.9 eV [151]. Dolocan experimentally found the bandgap of the tetragonal β-phase to be 2.6 eV and that of the ε-orthorhombic 2.85 eV [152].

With regard to the question whether *p*- or *n*-type conductivity prevails in Bi_2O_3, in the literature there are reports both for *n*- and *p*-type conductivity, depending on the fabrication method and parameters [149,153]. That allows to consider Bi_2O_3 as an amphoteric semiconductor [149]. Even for the same deposition technique, depending on the parameters, a changeover from *p* to *n*-type can arise. For instance, Morasch et al. [145], reported that films sputtered at lower O_2 content seem to have *n*-type character, but with increasing O_2 content the Fermi energy shifts lower within the bandgap, indicating a *p*-type character.

Bi_2O_3 has been applied in an ITO/Bi_2O_3/Au solar cell [145], with the rf magnetron-sputtered Bi_2O_3 films crystallizing in the β-phase for deposition temperature of 200°C, while amorphous films were obtained for room temperature deposition. The structure and the optical properties of the films depended on the deposition temperature and the amount of oxygen in the Ar/O_2 mixture. The bandgap of amorphous films was direct 3.3 eV and these films had a strong subgap absorption related to the presence of metallic particles. Textured films had a direct bandgap in the range of 2.5–2.8 eV. These values are too high for efficient light harvesting but ideal for water splitting. Depending on the deposition temperature, the V_{oc} varied from 0.530 to 0.683 V and the j_{sc} from 0.1 to 0.31 mA/cm^2, with the reported efficiency being 0.02%–0.05%.

11.6.3 Pb_xO_y Absorber

There is a plethora of lead-oxide compounds, and half a dozen of them have a stable crystal structure: tetragonal and orthorhombic modifications of both PbO (with oxidation state Pb^{II}) and PbO_2 (with oxidation state Pb^{IV}), and two mixed oxides, Pb_2O_3 and Pb_3O_4 (with oxidation state Pb^{II} and Pb^{IV}) [154]. Tetragonal PbO is a semiconductor with a forbidden bandgap of 1.9 eV, which rises to 2.4–2.8 eV in the case of the orthorhombic modification. The PbO_2 is also a semiconductor with a bandgap of 1.5–1.9 eV. Experimental values for the bandgap of Pb_3O_4 are between 2.1 and 2.2 eV [155]. PbO_2 and PbO are described as *n*-type semiconductors due to oxygen ion vacancies.

Droessler et al. fabricated Schottky junction solar cells based on tetragonal and orthorhombic PbO absorber with a bandgap between 2.2 and 2.4 eV. The solar cell architecture was glass/ITO/PbO/Al, with the authors claiming the formation of a Schottky junction at the PbO/Al interface. The maximum

achieved efficiency was 0.18% with $V_{oc} = 0.676$ V and $j_{sc} = 0.563$ mA/cm^2, achieved for thermally evaporated absorbers, post annealed at 270°C for 40 h [156].

11.6.4 Co_3O_4 Absorber

Co_3O_4 is the stable phase of the Co-O system at ambient temperature. It is a mixed valence compound [$Co^{II}Co_2^{III}O_4$] with a cubic spinel structure [157]. The stable phase of cobalt oxide above 300°C is CoO. While the CoO bandgap energy is around 5 eV [158] and therefore exceedingly high to be considered as solar absorber, the Co_3O_4 is a *p*-type semiconductor with experimentally obtained direct optical band gap value of 1.5 eV and another direct transition at about 2.0 eV, which were obtained for different deposition techniques [157,159–161]. It is produced by various techniques: RF sputtering, spray pyrolysis, chemical vapor deposition, or electrodeposition.

The appearance of two direct absorption transitions can be explained by the band structure of the material: the valence band has a strong 2*p* character, while the main contribution to the conduction band is from the Co^{II} 3*d* orbitals. The presence of Co^{III} in the oxide gives rise to a subband located inside the energy gap. So, the lower optical transition corresponds to the O $2p \rightarrow Co^{III}$ excitations, while the higher energy transition corresponds to the interband transitions defining the bandgap [157]. The acceptor level of CBD-grown films was estimated by Cheng et al. [159] at ~0.300 eV from the valence band, with a carrier concentration in the range of 2.45–2.79 10^{18} cm^{-3} ($T = 220$-400 K) and carrier mobility significantly smaller than 1 cm^2/Vs, indicating hopping conductance.

Kupfer et al. [162] have investigated an FTO/TiO_2/Co_3O_4/Au solar cell with TiO_2 window layer prepared by spray pyrolysis and Co_3O_4 solar absorber by PLD. The absorber presented a double optical transition of 1.5 and 2.2 eV. The photovoltaic performance was investigated as a function of the TiO_2 and the Co_3O_4 thickness, as well as of the Co_3O_4 deposition temperature. Best PV performance was obtained for Co_3O_4 thickness of 225 nm and deposition temperature of 600°C. Although a significant V_{oc} of 430 mV was achieved, the maximum j_{sc} was only about 200 μA/cm^2 and the efficiency 0.022%. In a later paper, the same group has reported j_{sc} up to 40 μA/cm^2 and similar V_{oc}, in a study where different metallic contacts (Ag, Cu, Ni, Co) were investigated and Ag was found to have the most favorable effect [163].

11.6.5 Fe_2O_3 Absorber

Hematite α-Fe_2O_3 is a semiconductor composed of nontoxic and abundant in nature elements. It crystallizes in the trigonal crystal system and is isostructural with corundum (α-Al_2O_3). The unit cell belongs to the R-3c space group and the α-phase is thermodynamically stable up to temperatures

of 1457°C [28] and also chemically stable at high pH values. The bandgap of hematite has been determined by various methods in the range of 1.9–2.3 eV, with some reports suggesting a direct type and others an indirect one [164]. The valence band of well-ordered, nearly stoichiometric hematite consists of O 2*p* and Fe 3*d* orbitals, which form a complicated structure about 10 eV wide [165]. The conduction band consists of Fe 3*d* orbitals [166]. The absorption coefficient of hematite increases abruptly at the bandgap energy and continues to increase for higher energies (with absorption in the order of $10^5\,cm^{-1}$), with marked absorption features centered at 2.4, 3.2, and 5.8 eV [167]. In the spectral region between 1.3 and 2.0 eV an absorption coefficient around $10^3\,cm^{-1}$ is obtained, with significant peaks at the 1.4–1.5 eV range [168]. This absorption was explained by spin-forbidden ligand field transitions between the Fe 3*d* states [168]. These states can be the origin of carrier recombination, reducing the minority carrier diffusion length.

There is a long debate in the literature whether hematite is a Mott-Hubbard insulator (where the band gap is defined by *d-d* transitions) or a charge-transfer insulator where the bandgap is formed between anion and cation states (O 2*p* → Fe 3*d*). However, the most recent experimental and theoretical results agree that α-Fe_2O_3 is a charge transfer insulator, with the valence band having a strong O 2*p* character [166,169–171]. Hematite has high resistivity (in the order of $10^6\,\Omega$ cm for single crystals), low electron mobility (0.01–0.1 cm^2/Vs), short hole diffusion length (2–4 nm) and high rate of carrier recombination ([164] and references therein). These disadvantages seem to hold independent of the preparation of the films and are the origin of the poor photoresponse of the material. In order to address the aforementioned issues, different approaches have been followed in the literature, such as to lower the resistivity through doping or employ Fe_2O_3 nanostructures to match the low diffusion length of minority carriers.

Hematite was used in so-called "wet-type solar cell" [172], where Fe_2O_3 thin films were deposited by laser ablation on an ITO- or FTO-coated glass and then calcinated at temperatures up to 800°C. Pt counter electrodes were sputtered on the same type of substrates. The two electrodes were then sandwiched and an electrolyte solution (KI/I_2) was filled between the two (Fe_2O_3 and Pt). Calcinated films at 700°C gave rise to solar cells with $V_{oc} = 290$ mV, $j_{sc} = 0.37$ mA/cm^2, and $\eta = 0.035\%$. Rühle et al. [173] reported an all-oxide solar cell of the structure FTO/ZnO/Fe_2O_3/Cr/Au with very low photocurrent in the order of a few μA/cm^2 and a $V_{oc} \approx 200$ mV, whereas the dark and light *I-V*s were not rectifying. The results clearly indicate the need for device optimization in order to achieve better PV performance with this absorber material.

In Table 11.2 we summarize the material properties of the main oxide absorbers, which have been implemented into solar cells in the literature. The table also shows the PV performance values for the best-performing cells.

TABLE 11.2 Material Properties of the Main Oxide Absorbers and Best Heterojunction Solar Cell Performance Figures Achieved so far With Each of the Absorbers

	CuO (tenorite)	**Co_3O_4**	**PbO_o (massicot)**	**PbO_t (litharge)**	**Fe_2O_3 (hematite)**	**β-Bi_2O_3**	**$BiFeO_3$**
Crystal system	Monoclinic	Cubic (spinel)	Orthorhombic	Tetragonal	Trigonal (corrundum)	Tetragonal	Trigonal
Space group	*C*2/*c*	$Fd\bar{3}m$	*Pbcm*	*P*4/*nmm*	$R\bar{3}c$	$P\bar{4}b2$	*R*3*c*
Bandgap (eV)	1.2–1.8	2.0	2.4–2.8	1.9	1.9–2.3	2.5–2.8	2.2–2.7
Conductivity type	*p*-type	*p*-type	*n*-type	*n*-type	Amphoteric	Amphoteric	Amphoteric
Best cell structure and performance							
Solar cell structure	Glass/ITO/CuO/$Zn_{90}Mg_{10}O$/Ag	Glass/FTO/TiO_2/Co_3O_4/Au	Glass/ITO/PbO (mixed PbO_o and PbO_t phases)/Al		Glass/FTO/ZnO/Fe_2O_3/Cr/Au	Glass/ITO/Bi_2O_3/Au	Glass/ITO/ZnO/BiFeO3/graphite
Deposition method of absorber	PLD	PLD	Thermal evaporation and post dep. annealing		PLD	RF magnetron sputtering	Spin coating of metal-organic precursor complex
η (%)	0.253	0.022	0.18		Negligible	0.02–0.05	3.98

Continued

TABLE 11.2 Material Properties of the Main Oxide Absorbers and Best Heterojunction Solar Cell Performance Figures Achieved so far With Each of the Absorbers—cont'd

	CuO (tenorite)	Co_3O_4	PbO_o (massicot)	PbO_t (litharge)	Fe_2O_3 (hematite)	β-Bi_2O_3	$BiFeO_3$
V_{oc} (V)	0.326	0.430	0.676		0.200	0.530–0.683	0.642
j_{sc} (mA/cm^2)	2.13	0.200	0.563		~0.006	0.10–0.31	12.47
Reference	2016, Bhardwaj et al. [143]	2015, Kupfer et al. [162]	2012, Droessler et al. [156]		2012, Rühle et al. [173]	2014, Morasch et al. [145]	2015, Tiwari et al. [173a]

11.7 FERROELECTRIC OXIDE SOLAR CELLS

In photovoltaic devices, the mechanism behind light conversion to electrical energy is the charge separation induced by the potential at a *p-n* junction. In the so-called ferroelectric photovoltaic effect (FEPV) the photo-generated carriers are transported by the polarization-induced internal electric field (also called depolarization field), present over the whole volume of a ferroelectric semiconducting material, within its domains and at the domain boundaries [174,175]. Due to this electric field, the photo-generated carriers can be efficiently separated, creating a net imbalance of their density near the domain walls and resulting in a band diagram, such as the one shown in Fig. 11.7 for a lateral device architecture. As the electric field is not localized at an interface (like in a *p-n* junction), but extends in the whole material, the charge transport through ferroelectrics is not diffusion-limited. Moreover, the generated photovoltages can attain values above-bandgap [175].

Typical ferroelectrics are oxides with the perovskite structure (ABO_3), such as the $LiNbO_3$, $Pb(Zr,Ti)O_3$ and $BiFeO_3$. In 2009, Choi et al. have reported a switchable ferroelectric diode and PV effect in $BiFeO_3$ films with semitransparent Au contacts. The diode effect was associated with the direction of the bulk electric polarization in the $BiFeO_3$, which could be flipped by an external voltage. $BiFeO_3$ contains transition metal ions with unpaired *d* electrons, giving rise to a relatively small optical bandgap (~2.2 eV) and high density of charged impurities and defects [175a]. In these devices, a bulk photocurrent density below 1 $\mu A/cm^2$ was reported [175b]. Until 2014, the conversion efficiency of FEPV cells remained extremely low, because of the low conductivity and the weak light absorption of FE semiconductors, as most of them have a high bandgap. Several attempts to lower the bandgap have been made in the literature but not without compromising the polarization of the material, leading to a net decrease of the FEPV performance. In 2014, Zheng et al. reported power conversion efficiency above 1% for a ferroelectric solar cell based on the $Pb(Zr,Ti)O_3$ (PZTO) film, which was combined with an a-Si layer to enhance the light absorption, in a perpendicular device of glass/ITO/PZTO/a-Si/Ag [176]. The appropriate band alignment between PZTO and a-Si guaranteed in this case efficient carrier transport within the device.

But the breakthrough in the FEPV came in the same year from Nechache et al. [177], who have managed to tune the $BiFeO_3$ bandgap by alloying the material with Cr. The bandgap of the resulting Bi_2FeCrO_6 (BFCO) perovskite could be tuned by means of the PLD growth and processing optimization, through the modification of the ordered/disordered phase ratio in the material. By stacking different layers of BFCO with bandgap values from 1.4 to 3.2 eV, one on top of the other, and using ITO as top transparent contact and niobium-doped $SrTiO_3$ as bottom contact, a broad part of the solar spectrum could be absorbed, giving rise to a dramatic enhancement of the PV performance, with reported values of: $j_{sc} = 20.6\,mA/cm^2$, $V_{oc} = 0.84\,V$ and $\eta = 8.1\%$ [177].

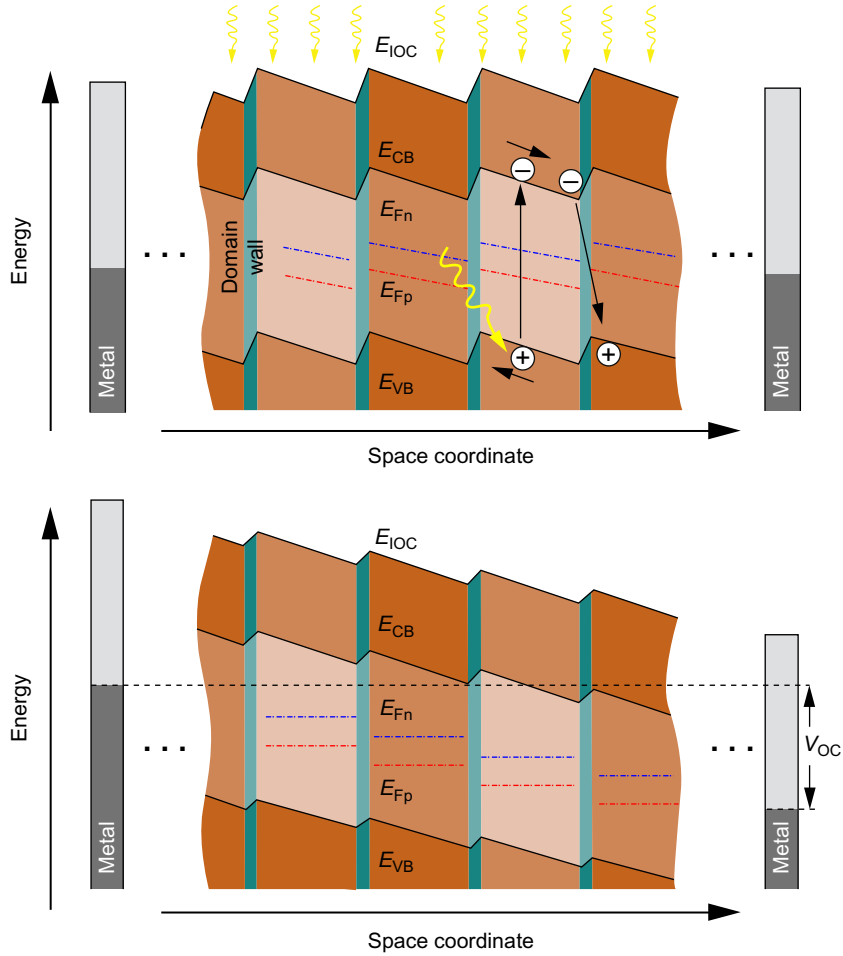

FIG. 11.7 Energy band diagram for ferroelectric solar cell at short (top) and open circuit (bottom) conditions, showing the ferroelectric domains and domain walls. Due to the lateral design, every domain is exposed to the light. The electrons and holes are transported towards the domain walls, where recombination takes place with carriers from the adjacent domain. As the different domains are connected in series, high open circuit voltages can be achieved. *(Reprinted with permission from S. Rühle et al., J. Phys. Chem. Lett. 3 (2012) 3755. Copyright 2012 American Chemical Society.)*

Finally, in 2015, Devendra Tiwari et al., used a conventional heterojunction architecture with a solution-processed $BiFeO_3$ absorber, deposited using the metal-organic precursor complex. The nanocrystalline absorber's bandgap was 2.2 eV, with absorption coefficient larger than $10^4\,cm^{-1}$. The authors fabricated solar cells of: glass/ITO/ZnO/$BiFeO_3$/graphite, yielding efficiency of 3.98%, with V_{oc}, j_{sc} and FF of 642 mV, 12.47 mA/cm^2 and 50.4%, respectively. How far the ferroelectric property of the absorber

influenced the cell performance (if at all) was not mentioned in this paper. Nevertheless, the reported cell performance is among the highest of all-oxide heterojunction solar cells [173a].

11.8 OUTLOOK

All-oxide solar cells have a promising future. In the last 10 years, advancements in the efficiency of cells based on Cu_2O, the most researched of the oxide absorbers, had an unprecedented rapid course. These advancements were driven mainly by the improvement of the *p-n* heterojunction quality, with the exploration of *n*-type materials that match the electronic band structure of the Cu_2O, as well as with the implementation of mild deposition techniques, such as pulsed laser deposition and atomic layer deposition, in order to create a defect-poor heterojunction interface.

The record power conversion efficiency today is more than 8%, while the open circuit voltage reaches beyond 1.1 V. The highest efficiency, however, is achieved using an energy- and material-intensive fabrication technique that is the thermal oxidation of copper sheets at high temperatures and long process durations. To enable the commercialization of all-oxide cells in the near future, a processing technique with low material and energy consumption, high-throughput and low investment costs, is necessary. The electrochemical deposition is a technique that fulfills these criteria. The state-of-the-art efficiency of electrodeposited-Cu_2O cells is today almost 4%, with a record open circuit voltage of 1.2 V. Although this value is half the one achieved with thermally oxidized Cu_2O, suggested technological improvements in the solar cell design and further optimization of the heterojunction, can boost the efficiency above the 10% target. Reaching this target can open the pathway to commercialization, given that the requirements of low-cost, low-toxicity, and long-term stability are met. Although single junction Cu_2O solar cells can be commercially exploitable, the future deployment of Cu_2O oxide cells includes tandem designs, in combination with other established or emerging, lower bandgap thin film absorbers, such as the CIGS or organohalide perovskites.

The development of heterojunction cells with other oxide absorbers is still at a very early stage to be able to evaluate their future role in the photovoltaics landscape. Most of these absorber materials have poor electronic properties. This issue can be mitigated by their implementation in nanostructured cell designs, in order to decouple the light absorption from the charge carrier transport. On the other hand, some of these oxides have polymorphs, each with very different electronic properties. This makes processing them challenging. Probably the most promising from this family of materials is the CuO, although still the highest reported efficiency is well below 1%.

For what concerns the ferroelectric oxides, the latest achievements on the perovskite $BiFeO_3$ absorber are very encouraging. The bandgap tuning of

this material through the alloying with Cr has enhanced the light absorption and led to an efficiency of 8.1% in graded bandgap ferroelectric PV cells. This high efficiency, combined with relatively simple cell design (which is not based on the heterojunction concept) make this type of cell very attractive. At the same time, the implementation of the $BiFeO_3$ Absorber in conventional heterojunction soalr cells also yielded efficiencies Close to 4%. These results demonstrate the great potential of oxide perovskite materials for future photovoltaics.

REFERENCES

[1] I.E.A. International Energy Agency, Key World Energy Statistics, OECD/IEA, Paris, France, 2016.
[2] N.S. Lewis, Powering the planet, MRS Bull. 32 (2007) 808–820.
[3] Solar Power Europe, Global Market Outlook for Solar Power/2016–2020, European Photovoltaic Industry Association, Brussels, 2016.
[4] C. Wadia, A.P. Alivisatos, D.M. Kammen, Materials availability expands the opportunity for large-scale photovoltaics deployment. Environ. Sci. Technol. 43 (2009) 2072–2077, https://doi.org/10.1021/es8019534.
[5] J. Jean, P.R. Brown, R.L. Jaffe, T. Buonassisi, V. Bulović, Pathways for solar photovoltaics. Energy Environ. Sci. 8 (2015) 1200–1219, https://doi.org/10.1039/C4EE04073B.
[6] T. Unold, H.W. Schock, Nonconventional (non-silicon-based) photovoltaic materials. Annu. Rev. Mater. Res. 41 (2011) 297–321, https://doi.org/10.1146/annurev-matsci-062910-100437.
[7] W. Shockley, H.J. Queisser, Detailed balance limit of efficiency of p-n junction solar cells. J. Appl. Phys. 32 (1961) 510, https://doi.org/10.1063/1.1736034.
[8] T. Gershon, Metal oxide applications in organic-based photovoltaics. Mater. Sci. Technol. 27 (2011) 1357–1371, https://doi.org/10.1179/026708311X13081465539809.
[9] M.T. Greiner, M.G. Helander, W.-M. Tang, Z.-B. Wang, J. Qiu, Z.-H. Lu, Universal energy-level alignment of molecules on metal oxides. Nat. Mater. 11 (2011) 76–81, https://doi.org/10.1038/nmat3159.
[10] J. Robertson, B. Falabretti, Band offsets of high K gate oxides on III-V semiconductors. J. Appl. Phys. 100 (2006) 14111, https://doi.org/10.1063/1.2213170.
[11] A. Imanishi, E. Tsuji, Y. Nakato, Dependence of the work function of TiO_2 (Rutile) on crystal faces, studied by a scanning auger microprobe. J. Phys. Chem. C 111 (2007) 2128–2132, https://doi.org/10.1021/jp0668403.
[12] A.L. Linsebigler, G. Lu, J.T. Yates, Photocatalysis on TiO_2 surfaces: principles, mechanisms, and selected results. Chem. Rev. 95 (1995) 735–758, https://doi.org/10.1021/cr00035a013.
[13] A. Klein, C. Körber, A. Wachau, F. Säuberlich, Y. Gassenbauer, S.P. Harvey, D.E. Proffit, T.O. Mason, Transparent conducting oxides for photovoltaics: manipulation of fermi level, work function and energy band alignment. Materials 3 (2010) 4892–4914, https://doi.org/10.3390/ma3114892.
[14] T. Minami, T. Miyata, T. Yamamoto, Work function of transparent conducting multicomponent oxide thin films prepared by magnetron sputtering. Surf. Coat. Technol. 108–109 (1998) 583–587, https://doi.org/10.1016/S0257-8972(98)00592-1.
[15] S. Gowtham, M. Deshpande, A. Costales, R. Pandey, Structural, energetic, electronic, bonding, and vibrational properties of Ga_3O, Ga_3O_2, Ga_3O_3, Ga_2O_3, and GaO_3 clusters. J. Phys. Chem. B 109 (2005) 14836–14844, https://doi.org/10.1021/jp050801u.

[16] F.P. Koffyberg, A photoelectrochemical determination of the position of the conduction and valence band edges of *p*-type CuO. J. Appl. Phys. 53 (1982) 1173, https://doi.org/10.1063/1.330567.
[17] L.C. Olsen, R.C. Bohara, M.W. Urie, Explanation for low-efficiency Cu_2O Schottky-barrier solar cells. Appl. Phys. Lett. 34 (1979) 47, https://doi.org/10.1063/1.90593.
[18] M. Kröger, S. Hamwi, J. Meyer, T. Riedl, W. Kowalsky, A. Kahn, Role of the deep-lying electronic states of MoO[sub 3] in the enhancement of hole-injection in organic thin films. Appl. Phys. Lett. 95 (2009) 123301, https://doi.org/10.1063/1.3231928.
[19] J. Meyer, K. Zilberberg, T. Riedl, A. Kahn, Electronic structure of Vanadium pentoxide: An efficient hole injector for organic electronic materials. J. Appl. Phys. 110 (2011) 33710, https://doi.org/10.1063/1.3611392.
[20] D.R. Lide (Ed.), CRC Handbook of Chemistry and Physics: A Ready-Reference Book of Chemical and Physical Data, 88th ed., CRC, Boca Raton, FL, 2008.
[21] A. Hagfeldt, Brief overview of dye-sensitized solar cells. AMBIO 41 (2012) 151–155, https://doi.org/10.1007/s13280-012-0272-7.
[22] M. Ye, X. Hong, F. Zhang, X. Liu, Recent advancements in perovskite solar cells: flexibility, stability and large scale. J. Mater. Chem. A 4 (2016) 6755–6771, https://doi.org/10.1039/C5TA09661H.
[23] A. Luque, A. Martí, Increasing the efficiency of ideal solar cells by photon induced transitions at intermediate levels. Phys. Rev. Lett. 78 (1997) 5014–5017, https://doi.org/10.1103/PhysRevLett.78.5014.
[24] D.S. Darvish, H.A. Atwater, Modeling, synthesis, and characterization of thin film copper oxide for solar cells. IEEE (2009) 002195–002199, https://doi.org/10.1109/PVSC.2009.5411394.
[25] L.O. Grondahl, Unidirectional current-carrying device, 1927. http://www.google.ch/patents/US1640335.
[26] B. Lange, Photoelements, Reinhold Publ. Corp., New York, 1938.
[27] B. Davydov, The rectifying action in semiconductors, Tech. Phys. USSR 5 (1938) 87.
[28] B. Davydov, On the photo-electromotive force in semiconductors, Tech. Phys. USSR 5 (1938) 79.
[29] N.F. Mott, The theory of crystal rectifiers, Proc. R. Soc. Lond. 171 (1939) 27.
[30] W. Schottky, Zur Halbleitertheorie der Sperrschicht- und Spitzengleichrichter. Z. Für Phys. (1939) 367–414, https://doi.org/10.1007/BF01340116.
[31] D.M. Chapin, C.S. Fuller, G.L. Pearson, A new silicon p-n junction photocell for converting solar radiation into electrical power. J. Appl. Phys. 25 (1954) 676, https://doi.org/10.1063/1.1721711.
[32] D. Trivitch, E.Y. Wang, R.J. Komp, A.S. Kakar, Cuprous oxide photovoltaic cells, in: Proc. 13th IEEE Photovolt. Spec. Conf. Wash., DC, 1978. 174.
[33] L.C. Olsen, F.W. Addis, W. Miller, Experimental and theoretical studies of Cu_2O solar cells. Sol. Cells 7 (1982) 247–279, https://doi.org/10.1016/0379-6787(82)90050-3.
[34] A. Musa, T. Akomolafe, M. Carter, Production of cuprous oxide, a solar cell material, by thermal oxidation and a study of its physical and electrical properties. Sol. Energy Mater. Sol. Cells 51 (1998) 305–316, https://doi.org/10.1016/S0927-0248(97)00233-X.
[35] T.D. Golden, M.G. Shumsky, Y. Zhou, R.A. VanderWerf, R.A. Van Leeuwen, J.A. Switzer, Electrochemical deposition of copper(I) oxide films. Chem. Mater. 8 (1996) 2499–2504, https://doi.org/10.1021/cm9602095.
[36] M. Pavan, S. Rühle, A. Ginsburg, D.A. Keller, H.-N. Barad, P.M. Sberna, D. Nunes, R. Martins, A.Y. Anderson, A. Zaban, E. Fortunato, TiO_2/Cu_2O all-oxide heterojunction solar cells produced by spray pyrolysis. Sol. Energy Mater. Sol. Cells 132 (2015) 549–556, https://doi.org/10.1016/j.solmat.2014.10.005.

[37] Y. Ashworth, The anodic formation of Cu[sub 2]O in alkaline solutions. J. Electrochem. Soc. 124 (1977) 506, https://doi.org/10.1149/1.2133338.
[38] M. Ristov, G. Sinadinovski, M. Mitreski, Chemically deposited Cu_2O thin film as an oxygen pressure sensor. Thin Solid Films 167 (1988) 309–316, https://doi.org/10.1016/0040-6090(88)90508-1.
[39] N. Soundaram, R. Chandramohan, S. Valanarasu, R. Thomas, A. Kathalingam, Studies on SILAR deposited Cu_2O and ZnO films for solar cell applications. J. Mater. Sci. Mater. Electron. 26 (2015) 5030–5036, https://doi.org/10.1007/s10854-015-3020-5.
[40] S. Chatterjee, S.K. Saha, A.J. Pal, Formation of all-oxide solar cells in atmospheric condition based on Cu_2O thin-films grown through SILAR technique. Sol. Energy Mater. Sol. Cells 147 (2016) 17–26, https://doi.org/10.1016/j.solmat.2015.11.045.
[41] C. Ortiz, C.N. Afonso, F. Vega, J. Solis, J.C. Cheang, C. Ortega, J. Siejka, Laser deposition of copper oxide thin films: contrast with sputtering. Appl. Surf. Sci. 54 (1992) 201–204, https://doi.org/10.1016/0169-4332(92)90044-X.
[42] M.F. Al-Kuhaili, Characterization of copper oxide thin films deposited by the thermal evaporation of cuprous oxide (Cu_2O). Vacuum 82 (2008) 623–629, https://doi.org/10.1016/j.vacuum.2007.10.004.
[43] L.S. Hong, H. Komiyama, Chemical vapor deposition of CuO*x* films by CuI and O_2: role of cluster formation on film morphology. J. Am. Ceram. Soc. 74 (1991) 1597–1604, https://doi.org/10.1111/j.1151-2916.1991.tb07145.x.
[44] S. Ishizuka, T. Maruyama, K. Akimoto, Thin-film deposition of Cu_2O by reactive radio-frequency magnetron sputtering, Jpn. J. Appl. Phys. 39 (2000) L786–L788.
[45] K. Momma, F. Izumi, VESTA 3 for three-dimensional visualization of crystal, volumetric and morphology data, J. Appl. Cryst. 44 (2011) 1272–1276.
[46] H. Raebiger, S. Lany, A. Zunger, Origins of the *p*-type nature and cation deficiency in Cu_2O and related materials. Phys. Rev. B 76 (2007) https://doi.org/10.1103/PhysRevB.76.045209.
[47] A. Soon, X.Y. Cui, B. Delley, S.-H. Wei, C. Stampfl, Native defect-induced multifarious magnetism in nonstoichiometric cuprous oxide: first-principles study of bulk and surface properties of $Cu_{2-\delta}O$. Phys. Rev. B 79 (2009) https://doi.org/10.1103/PhysRevB.79.035205.
[48] O. Porat, I. Riess, Defect chemistry of $Cu_{2-y}O$ at elevated temperatures. Part I: non-stoichiometry, phase width and dominant point defects. Solid State Ion 74 (1994) 229–238, https://doi.org/10.1016/0167-2738(94)90215-1.
[49] B.K. Meyer, A. Polity, D. Reppin, M. Becker, P. Hering, P.J. Klar, T. Sander, C. Reindl, J. Benz, M. Eickhoff, C. Heiliger, M. Heinemann, J. Bläsing, A. Krost, S. Shokovets, C. Müller, C. Ronning, Binary copper oxide semiconductors: from materials towards devices. Phys. Status Solidi B 249 (2012) 1487–1509, https://doi.org/10.1002/pssb.201248128.
[50] M. Nolan, S.D. Elliott, The *p*-type conduction mechanism in Cu_2O: a first principles study. Phys. Chem. Chem. Phys. 8 (2006) 5350, https://doi.org/10.1039/b611969g.
[51] A. Mittiga, E. Salza, F. Sarto, M. Tucci, R. Vasanthi, Heterojunction solar cell with 2% efficiency based on a Cu[sub 2]O substrate. Appl. Phys. Lett. 88 (2006) 163502, https://doi.org/10.1063/1.2194315.
[52] F. Biccari, C. Malerba, A. Mittiga, Chlorine doping of Cu_2O. Sol. Energy Mater. Sol. Cells 94 (2010) 1947–1952, https://doi.org/10.1016/j.solmat.2010.06.022.
[53] C. Malerba, F. Biccari, C. Leonor Azanza Ricardo, M. D'Incau, P. Scardi, A. Mittiga, Absorption coefficient of bulk and thin film Cu_2O. Sol. Energy Mater. Sol. Cells 95 (2011) 2848–2854, https://doi.org/10.1016/j.solmat.2011.05.047.

[54] Y. Liu, H.K. Turley, J.R. Tumbleston, E.T. Samulski, R. Lopez, Minority carrier transport length of electrodeposited Cu[sub 2]O in ZnO/Cu[sub 2]O heterojunction solar cells. Appl. Phys. Lett. 98 (2011) 162105, https://doi.org/10.1063/1.3579259.

[55] S. Ishizuka, S. Kato, T. Maruyama, K. Akimoto, Nitrogen doping into Cu_2O thin films deposited by reactive radio-frequency magnetron sputtering. Jpn. J. Appl. Phys. 40 (2001) 2765–2768, https://doi.org/10.1143/JJAP.40.2765.

[56] Y. Nakano, S. Saeki, T. Morikawa, Optical bandgap widening of *p*-type Cu[sub 2]O films by nitrogen doping. Appl. Phys. Lett. 94 (2009) 22111, https://doi.org/10.1063/1.3072804.

[57] Z. Zang, A. Nakamura, J. Temmyo, Nitrogen doping in cuprous oxide films synthesized by radical oxidation at low temperature. Mater. Lett. 92 (2013) 188–191, https://doi.org/10.1016/j.matlet.2012.10.083.

[58] C. Malerba, C.L. Azanza Ricardo, M. D'Incau, F. Biccari, P. Scardi, A. Mittiga, Nitrogen doped Cu_2O: a possible material for intermediate band solar cells? Sol. Energy Mater. Sol. Cells 105 (2012) 192–195, https://doi.org/10.1016/j.solmat.2012.06.017.

[59] S. Ishizuka, S. Kato, Y. Okamoto, K. Akimoto, Control of hole carrier density of polycrystalline Cu[sub 2]O thin films by Si doping. Appl. Phys. Lett. 80 (2002) 950, https://doi.org/10.1063/1.1448398.

[60] B. Heng, T. Xiao, W. Tao, X. Hu, X. Chen, B. Wang, D. Sun, Y. Tang, Zn doping-induced shape evolution of microcrystals: the case of cuprous oxide. Cryst. Growth Des. 12 (2012) 3998–4005, https://doi.org/10.1021/cg3004799.

[61] Y. Zhang, L. Pan, H. Zhu, H. Qiu, J. Yin, Y. Li, F. Zhao, X. Zhao, J.Q. Xiao, Fabrication and characterization of Mn-doped Cu_2O thin films grown by RF magnetron sputtering, J. Magn. Magn. Mater. 320 (2008) 3303–3306, https://doi.org/10.1016/j.jmmm.2008.06.035.

[62] N. Kikuchi, K. Tonooka, Electrical and structural properties of Ni-doped Cu_2O films prepared by pulsed laser deposition. Thin Solid Films 486 (2005) 33–37, https://doi.org/10.1016/j.tsf.2004.12.044.

[63] N. Kikuchi, K. Tonooka, E. Kusano, Mechanisms of carrier generation and transport in Ni-doped Cu_2O. Vacuum 80 (2006) 756–760, https://doi.org/10.1016/j.vacuum.2005.11.039.

[64] L. Bergerot, C. Jiménez, O. Chaix-Pluchery, L. Rapenne, J.-L. Deschanvres, Growth and characterization of Sr-doped Cu_2O thin films deposited by metalorganic chemical vapor deposition: growth and characterization of Sr-doped Cu_2O thin films. Phys. Status Solidi A 212 (2015) 1735–1741, https://doi.org/10.1002/pssa.201431750.

[65] T. Minami, Y. Nishi, T. Miyata, Heterojunction solar cell with 6% efficiency based on an *n*-type aluminum-gallium-oxide thin film and *p*-type sodium-doped Cu_2O sheet. Appl. Phys. Express. 8 (2015) 22301, https://doi.org/10.7567/APEX.8.022301.

[66] Y. Tsur, I. Riess, Self-compensation in semiconductors. Phys. Rev. B 60 (1999) 8138–8146, https://doi.org/10.1103/PhysRevB.60.8138.

[67] A. Martínez-Ruiz, M.G. Moreno, N. Takeuchi, First principles calculations of the electronic properties of bulk Cu_2O, clean and doped with Ag, Ni, and Zn. Solid State Sci. 5 (2003) 291–295, https://doi.org/10.1016/S1293-2558(03)00003-7.

[68] T. Minami, Y. Nishi, T. Miyata, Impact of incorporating sodium into polycrystalline *p*-type Cu_2O for heterojunction solar cell applications. Appl. Phys. Lett. 105 (2014) 212104, https://doi.org/10.1063/1.4902879.

[69] W. Siripala, J.R.P. Jayakody, Observation of *n*-type photoconductivity in electrodeposited copper oxide film electrodes in a photoelectrochemical cell. Sol. Energy Mater. 14 (1986) 23–27, https://doi.org/10.1016/0165-1633(86)90010-9.

[70] C. Jayewardena, K.P. Hewaparakrama, D.L.A. Wijewardena, H. Guruge, Fabrication of n-Cu_2O electrodes with higher energy conversion efficiency in a photoelectrochemical cell. Sol. Energy Mater. Sol. Cells 56 (1998) 29–33, https://doi.org/10.1016/S0927-0248(98)00104-4.

[71] C.A. Fernando, S. Wetthasinghe, Investigation of photoelectrochemical characteristics of *n*-type Cu_2O films. Sol. Energy Mater. Sol. Cells 63 (2000) 299–308, https://doi.org/10.1016/S0927-0248(00)00036-2.

[72] R. Garuthara, W. Siripala, Photoluminescence characterization of polycrystalline *n*-type Cu_2O films. J. Lumin. 121 (2006) 173–178, https://doi.org/10.1016/j.jlumin.2005.11.010.

[73] L. Wang, M. Tao, Fabrication and characterization of p-n homojunctions in cuprous oxide by electrochemical deposition. Electrochem. Solid-State Lett. 10 (2007) H248, https://doi.org/10.1149/1.2748632.

[74] K. Han, M. Tao, Electrochemically deposited p-n homojunction cuprous oxide solar cells. Sol. Energy Mater. Sol. Cells 93 (2009) 153–157, https://doi.org/10.1016/j.solmat.2008.09.023.

[75] M.-J. Hong, Y.-C. Lin, L.-C. Chao, P.-H. Lin, B.-R. Huang, Cupric and cuprous oxide by reactive ion beam sputter deposition and the photosensing properties of cupric oxide metal-semiconductor-metal Schottky photodiodes. Appl. Surf. Sci. 346 (2015) 18–23, https://doi.org/10.1016/j.apsusc.2015.03.185.

[76] D.O. Scanlon, G.W. Watson, Undoped *n*-type Cu_2O: fact or fiction? J. Phys. Chem. Lett. 1 (2010) 2582–2585, https://doi.org/10.1021/jz100962n.

[77] J.-N. Nian, C.-C. Tsai, P.-C. Lin, H. Teng, Elucidating the conductivity-type transition mechanism of *p*-type Cu[sub 2]O films from electrodeposition. J. Electrochem. Soc. 156 (2009) H567, https://doi.org/10.1149/1.3125800.

[78] J.A. Assimos, Photovoltaic properties and barrier heights of single-crystal and polycrystalline Cu_2O[single bond]Cu contacts. J. Appl. Phys. 44 (1973) 1687, https://doi.org/10.1063/1.1662432.

[79] R.J. Iwanowski, D. Trivich†dr, Enhancement of the photovoltaic conversion efficiency in Cu/Cu_2O schottky barrier solar cells by H^+ ion irradiation. Phys. Status Solidi A 95 (1986) 735–741, https://doi.org/10.1002/pssa.2210950244.

[80] L. Papadimitriou, N.A. Economou, D. Trivich, Heterojunction solar cells on cuprous oxide. Sol. Cells 3 (1981) 73–80, https://doi.org/10.1016/0379-6787(81)90084-3.

[81] J. Herion, E.A. Niekisch, G. Scharl, Investigation of metal oxide/cuprous oxide heterojunction solar cells. Sol. Energy Mater. 4 (1980) 101–112, https://doi.org/10.1016/0165-1633(80)90022-2.

[82] T. Minami, T. Miyata, K. Ihara, Y. Minamino, S. Tsukada, Effect of ZnO film deposition methods on the photovoltaic properties of ZnO-Cu_2O heterojunction devices. Thin Solid Films 494 (2006) 47–52, https://doi.org/10.1016/j.tsf.2005.07.167.

[83] T. Minami, Y. Nishi, T. Miyata, J. Nomoto, High-efficiency oxide solar cells with ZnO/Cu_2O heterojunction fabricated on thermally oxidized Cu_2O sheets. Appl. Phys. Express 4 (2011) 62301, https://doi.org/10.1143/APEX.4.062301.

[84] Y. Nishi, T. Miyata, T. Minami, The impact of heterojunction formation temperature on obtainable conversion efficiency in n-ZnO/p-Cu_2O solar cells. Thin Solid Films 528 (2013) 72–76, https://doi.org/10.1016/j.tsf.2012.09.090.

[85] B. Kramm, A. Laufer, D. Reppin, A. Kronenberger, P. Hering, A. Polity, B.K. Meyer, The band alignment of Cu_2O/ZnO and Cu2O/GaN heterostructures. Appl. Phys. Lett. 100 (2012) 94102, https://doi.org/10.1063/1.3685719.

[86] A. Ohtomo, M. Kawasaki, T. Koida, K. Masubuchi, H. Koinuma, Y. Sakurai, Y. Yoshida, T. Yasuda, Y. Segawa, Mg[sub x]Zn[sub $1-x$]O as a II–VI widegap semiconductor alloy. Appl. Phys. Lett. 72 (1998) 2466, https://doi.org/10.1063/1.121384.

[87] A. Suryanarayana Reddy, P. Prathap, Y.P.V. Subbaiah, K.T. Ramakrishna Reddy, J. Yi, Growth and physical behaviour of $Zn_{1-x}Mg_xO$ films. Thin Solid Films 516 (2008) 7084–7087, https://doi.org/10.1016/j.tsf.2007.12.098.

[88] A. Kaushal, D. Kaur, Effect of Mg content on structural, electrical and optical properties of $Zn_{1-x}Mg_xO$ nanocomposite thin films. Sol. Energy Mater. Sol. Cells 93 (2009) 193–198, https://doi.org/10.1016/j.solmat.2008.09.039.

[89] André Bikowski, The Relation Between the Deposition Process and the Structural, Electronic, and Transport Properties of Magnetron Sputtered Doped ZnO and $Zn_{1-x}Mg_xO$ Films, Mathematisch-Naturwissenschaftlichen Fakultät I der Humboldt- Universität zu Berlin, Berlin, 2014.

[90] T. Minami, Y. Nishi, T. Miyata, S. Abe, Photovoltaic properties in Al-doped ZnO/non-doped $Zn_{1-x}Mg_xO/Cu_2O$ heterojunction solar cells. ECS Trans. 50 (2013) 59–68, https://doi.org/10.1149/05051.0059ecst.

[91] Y. Xu, M.A.A. Schoonen, The absolute energy positions of conduction and valence bands of selected semiconducting minerals, Am. Miner. (2000) 543–556.

[92] T. Minami, Y. Nishi, T. Miyata, High-efficiency Cu_2O-based heterojunction solar cells fabricated using a Ga_2O_3 thin film as n-type layer. Appl. Phys. Express. 6 (2013) 44101, https://doi.org/10.7567/APEX.6.044101.

[93] K. Oishi, Y. Matsuo, Internal photoemission and photoconduction on films. Thin Solid Films 274 (1996) 133–137, https://doi.org/10.1016/0040-6090(95)07093-1.

[94] H. Kim, C. Jin, S. Park, Y. Kwon, S. Lee, C. Lee, Influence of ZnO encapsulation on the luminescence property of GeO_2 nanowires. Phys. Scr. T149 (2012) 14052, https://doi.org/10.1088/0031-8949/2012/T149/014052.

[95] V.V. Afanas'ev, A. Stesmans, Energy band alignment at the (100)Ge/HfO[sub 2] interface. Appl. Phys. Lett. 84 (2004) 2319, https://doi.org/10.1063/1.1688453.

[96] T. Minami, Y. Nishi, T. Miyata, Cu_2O-based solar cells using oxide semiconductors. J. Semicond. 37 (2016) 14002, https://doi.org/10.1088/1674-4926/37/1/014002.

[97] T. Minami, Y. Nishi, T. Miyata, Efficiency enhancement using a $Zn_{1-x}Ge_x$-O thin film as an n-type window layer in Cu_2O-based heterojunction solar cells. Appl. Phys. Express. 9 (2016) 52301, https://doi.org/10.7567/APEX.9.052301.

[98] O. Ergen, A. Gibb, O. Vazquez-Mena, W.R. Regan, A. Zettl, Metal insulator semiconductor solar cell devices based on a Cu_2O substrate utilizing h-BN as an insulating and passivating layer. Appl. Phys. Lett. 106 (2015) 103904, https://doi.org/10.1063/1.4914181.

[99] T. Mahalingam, J.S.P. Chitra, J.P. Chu, S. Velumani, P.J. Sebastian, Structural and annealing studies of potentiostatically deposited Cu_2O thin films. Sol. Energy Mater. Sol. Cells 88 (2005) 209–216, https://doi.org/10.1016/j.solmat.2004.05.026.

[100] J. Cui, U.J. Gibson, A simple two-step electrodeposition of Cu_2O/ZnO nanopillar solar cells. J. Phys. Chem. C 114 (2010) 6408–6412, https://doi.org/10.1021/jp1004314.

[101] W. Septina, S. Ikeda, M.A. Khan, T. Hirai, T. Harada, M. Matsumura, L.M. Peter, Potentiostatic electrodeposition of cuprous oxide thin films for photovoltaic applications. Electrochim. Acta 56 (2011) 4882–4888, https://doi.org/10.1016/j.electacta.2011.02.075.

[102] S. Hussain, C. Cao, Z. Usman, Z. Chen, G. Nabi, W.S. Khan, Z. Ali, F.K. Butt, T. Mahmood, Fabrication and photovoltaic characteristics of Cu_2O/TiO_2 thin film heterojunction solar cell. Thin Solid Films 522 (2012) 430–434, https://doi.org/10.1016/j.tsf.2012.08.013.

[103] G. Guerguerian, F. Elhordoy, C.J. Pereyra, R.E. Marotti, F. Martín, D. Leinen, J.R. Ramos-Barrado, E.A. Dalchiele, ZnO/Cu_2O heterostructure nanopillar arrays: synthesis, structural and optical properties. J. Phys. Appl. Phys. 45 (2012) 245301, https://doi.org/10.1088/0022-3727/45/24/245301.

[104] A.S. Zoolfakar, R.A. Rani, A.J. Morfa, S. Balendhran, A.P. O'Mullane, S. Zhuiykov, K. Kalantar-zadeh, Enhancing the current density of electrodeposited ZnO-Cu_2O solar cells by engineering their heterointerfaces. J. Mater. Chem. 22 (2012) 21767, https://doi.org/10.1039/c2jm35682a.

[105] T. Dimopoulos, A. Peić, S. Abermann, M. Postl, E.J.W. List-Kratochvil, R. Resel, Effect of thermal annealing in vacuum on the photovoltaic properties of electrodeposited Cu_2O-absorber solar cell. EPJ Photovolt. 5 (2014) 50301, https://doi.org/10.1051/epjpv/2014005.

[106] J. Katayama, K. Ito, M. Matsuoka, J. Tamaki, Performance of Cu_2O/ZnO solar cell prepared by two-step electrodeposition. J. Appl. Electrochem. 34 (2004) 687–692, https://doi.org/10.1023/B:JACH.0000031166.73660.c1.

[107] M. Izaki, T. Shinagawa, K.-T. Mizuno, Y. Ida, M. Inaba, A. Tasaka, Electrochemically constructed p-Cu_2O/*n*-ZnO heterojunction diode for photovoltaic device. J. Phys. Appl. Phys. 40 (2007) 3326–3329, https://doi.org/10.1088/0022-3727/40/11/010.

[108] S.S. Jeong, A. Mittiga, E. Salza, A. Masci, S. Passerini, Electrodeposited ZnO/Cu_2O heterojunction solar cells. Electrochim. Acta 53 (2008) 2226–2231, https://doi.org/10.1016/j.electacta.2007.09.030.

[109] K.P. Musselman, A. Wisnet, D.C. Iza, H.C. Hesse, C. Scheu, J.L. MacManus-Driscoll, L. Schmidt-Mende, Strong efficiency improvements in ultra-low-cost inorganic nanowire solar cells. Adv. Mater. 22 (2010) E254–E258, https://doi.org/10.1002/adma.201001455.

[110] Y.S. Lee, J. Heo, S.C. Siah, J.P. Mailoa, R.E. Brandt, S.B. Kim, R.G. Gordon, T. Buonassisi, Ultrathin amorphous zinc-tin-oxide buffer layer for enhancing heterojunction interface quality in metal-oxide solar cells. Energy Environ. Sci. 6 (2013) 2112, https://doi.org/10.1039/c3ee24461j.

[111] S.W. Lee, Y.S. Lee, J. Heo, S.C. Siah, D. Chua, R.E. Brandt, S.B. Kim, J.P. Mailoa, T. Buonassisi, R.G. Gordon, Improved Cu_2O-based solar cells using atomic layer deposition to control the Cu oxidation state at the p-n junction. Adv. Energy Mater. 4 (2014) 1301916, https://doi.org/10.1002/aenm.201301916.

[112] Y.S. Lee, D. Chua, R.E. Brandt, S.C. Siah, J.V. Li, J.P. Mailoa, S.W. Lee, R.G. Gordon, T. Buonassisi, Atomic layer deposited gallium oxide buffer layer enables 1.2V open-circuit voltage in cuprous oxide solar cells. Adv. Mater. 26 (2014) 4704–4710, https://doi.org/10.1002/adma.201401054.

[113] R.E. Brandt, M. Young, H.H. Park, A. Dameron, D. Chua, Y.S. Lee, G. Teeter, R.G. Gordon, T. Buonassisi, Band offsets of *n*-type electron-selective contacts on cuprous oxide (Cu_2O) for photovoltaics. Appl. Phys. Lett. 105 (2014) 263901, https://doi.org/10.1063/1.4905180.

[114] J. Kaur, O. Bethge, R.A. Wibowo, N. Bansal, M. Bauch, R. Hamid, E. Bertagnolli, T. Dimopoulos, All-oxide solar cells based on electrodeposited Cu<ce:inf>2</ce:inf>O absorber and atomic layer deposited ZnMgO on precious-metal-free electrode Sol. Energy Mater. Sol. Cells 161 (2017) 449–459, https://doi.org/10.1016/j.solmat.2016.12.017.

[115] Z. Duan, A.Du. Pasquier, Y. Lu, Y. Xu, E. Garfunkel, Effects of Mg composition on open circuit voltage of Cu_2O-$Mg_xZn_{1-x}O$ heterojunction solar cells. Sol. Energy Mater. Sol. Cells 96 (2012) 292–297, https://doi.org/10.1016/j.solmat.2011.09.047.

[116] S.H. Wee, P.-S. Huang, J.-K. Lee, A. Goyal, Heteroepitaxial Cu_2O thin film solar cell on metallic substrates. Sci. Rep. 5 (2015) 16272, https://doi.org/10.1038/srep16272.

[117] C.-L. Kuo, R.-C. Wang, J.-L. Huang, C.-P. Liu, C.-K. Wang, S.-P. Chang, W.-H. Chu, C.-H. Wang, C. Tu, The synthesis and electrical characterization of Cu_2O/Al:ZnO radial p–n junction nanowire arrays. Nanotechnology 20 (2009) 365603, https://doi.org/10.1088/0957-4484/20/36/365603.

[118] B.D. Yuhas, P. Yang, Nanowire-based all-oxide solar cells. J. Am. Chem. Soc. 131 (2009) 3756–3761, https://doi.org/10.1021/ja8095575.

[119] K.P. Musselman, A. Marin, L. Schmidt-Mende, J.L. MacManus-Driscoll, Incompatible length scales in nanostructured Cu_2O solar cells. Adv. Funct. Mater. 22 (2012) 2202–2208, https://doi.org/10.1002/adfm.201102263.

[120] S.K. Baek, K.R. Lee, H.K. Cho, Oxide p-n Heterojunction of Cu_2O/ZnO nanowires and their photovoltaic performance. J. Nanomater. 2013 (2013) 1–7, https://doi.org/10.1155/2013/421371.

[121] Y.-S. Chen, C.-H. Liao, Y.-L. Chueh, C.-C. Lai, L.-Y. Chen, A.-K. Chu, C.-T. Kuo, H.-C. Wang, High performance Cu_2O/ZnO core-shell nanorod arrays synthesized using a nanoimprint GaN template by the hydrothermal growth technique. Opt. Mater. Express. 4 (2014) 1473, https://doi.org/10.1364/OME.4.001473.

[122] M. Abd-Ellah, J.P. Thomas, L. Zhang, K.T. Leung, Enhancement of solar cell performance of p-Cu_2O/n-ZnO-nanotube and nanorod heterojunction devices. Sol. Energy Mater. Sol. Cells 152 (2016) 87–93, https://doi.org/10.1016/j.solmat.2016.03.022.

[123] L. Wang, Y. Zhao, G. Wang, H. Zhou, C. Geng, C. Wu, J. Xu, Enhancing the efficiency of ZnO/Cu_2O inorganic nanostructure solar cells simply by CdS quantum dots. Sol. Energy Mater. Sol. Cells 130 (2014) 387–392, https://doi.org/10.1016/j.solmat.2014.07.027.

[124] L. Zhang, H. Sun, L. Xie, J. Lu, L. Zhang, S. Wu, X. Gao, X. Lu, J. Li, J.-M. Liu, Inorganic solar cells based on electrospun ZnO nanofibrous networks and electrodeposited Cu_2O. Nanoscale Res. Lett. 10 (2015) https://doi.org/10.1186/s11671-015-1169-8.

[125] D. Li, C.-J. Chien, S. Deora, P.-C. Chang, E. Moulin, J.G. Lu, Prototype of a scalable core-shell Cu_2O/TiO_2 solar cell. Chem. Phys. Lett. 501 (2011) 446–450, https://doi.org/10.1016/j.cplett.2010.11.064.

[126] C.M. McShane, W.P. Siripala, K.-S. Choi, Effect of junction morphology on the performance of polycrystalline Cu_2O homojunction solar cells. J. Phys. Chem. Lett. 1 (2010) 2666–2670, https://doi.org/10.1021/jz100991e.

[127] L. Xiong, S. Huang, X. Yang, M. Qiu, Z. Chen, Y. Yu, *p*-Type and *n*-type Cu_2O semiconductor thin films: controllable preparation by simple solvothermal method and photoelectrochemical properties. Electrochim. Acta 56 (2011) 2735–2739, https://doi.org/10.1016/j.electacta.2010.12.054.

[128] C.M. McShane, K.-S. Choi, Junction studies on electrochemically fabricated p–n Cu_2O homojunction solar cells for efficiency enhancement. Phys. Chem. Chem. Phys. 14 (2012) 6112, https://doi.org/10.1039/c2cp40502d.

[129] Y.-K. Hsu, J.-R. Wu, M.-H. Chen, Y.-C. Chen, Y.-G. Lin, Fabrication of homojunction Cu_2O solar cells by electrochemical deposition. Appl. Surf. Sci. 354 (2015) 8–13, https://doi.org/10.1016/j.apsusc.2015.05.142.

[130] L. Yu, L. Xiong, Y. Yu, Cu_2O homojunction solar cells: F-doped *n*-type thin film and highly improved efficiency. J. Phys. Chem. C 119 (2015) 22803–22811, https://doi.org/10.1021/acs.jpcc.5b06736.

[131] T. Minami, N. Yuki, T. Miyata, A. Shinya, Photovoltaic properties in Al-doped ZnO/non-doped $Zn_{1-x}Mg_xO/Cu_2O$ heterojunction solar cells, Honol. PRiME 2012 (2012).

[132] Y. Ievskaya, R.L.Z. Hoye, A. Sadhanala, K.P. Musselman, J.L. MacManus-Driscoll, Fabrication of ZnO/Cu_2O heterojunctions in atmospheric conditions: improved interface quality and solar cell performance. Sol. Energy Mater. Sol. Cells 135 (2015) 43–48, https://doi.org/10.1016/j.solmat.2014.09.018.

[133] S. Åsbrink, L.J. Norrby, A refinement of the crystal structure of copper(II) oxide with a discussion of some exceptional e.s.d'.s. Acta Crystallogr. B 26 (1970) 8–15, https://doi.org/10.1107/S0567740870001838.

[134] D. Wu, Q. Zhang, M. Tao, LSDA + U study of cupric oxide: electronic structure and native point defects. Phys. Rev. B 73 (2006), https://doi.org/10.1103/PhysRevB.73.235206.

[135] S.C. Ray, Preparation of copper oxide thin film by the sol-gel-like dip technique and study of their structural and optical properties. Sol. Energy Mater. Sol. Cells 68 (2001) 307–312, https://doi.org/10.1016/S0927-0248(00)00364-0.

[136] K.L. Hardee, Semiconductor electrodes. J. Electrochem. Soc. 124 (1977) 215, https://doi.org/10.1149/1.2133269.

[137] T. Dimopoulos, A. Peić, P. Müllner, M. Neuschitzer, R. Resel, S. Abermann, M. Postl, E.J.W. List, S. Yakunin, W. Heiss, H. Brückl, Photovoltaic properties of thin film heterojunctions with cupric oxide absorber. J. Renew. Sustain. Energy 5 (2013) 11205, https://doi.org/10.1063/1.4791779.

[138] S. Masudy-Panah, K. Radhakrishnan, H.R. Tan, R. Yi, T.I. Wong, G.K. Dalapati, Titanium doped cupric oxide for photovoltaic application. Sol. Energy Mater. Sol. Cells 140 (2015) 266–274, https://doi.org/10.1016/j.solmat.2015.04.024.

[139] J. Morasch, H.F. Wardenga, W. Jaegermann, A. Klein, Influence of grain boundaries and interfaces on the electronic structure of polycrystalline CuO thin films: grain boundaries and interfaces of polycrystalline CuO thin films. Phys. Status Solidi A 213 (2016) 1615–1624, https://doi.org/10.1002/pssa.201533018.

[140] M. Heinemann, B. Eifert, C. Heiliger, Band structure and phase stability of the copper oxides Cu_2O, CuO, and Cu_4O_3. Phys. Rev. B 87 (2013) https://doi.org/10.1103/PhysRevB.87.115111.

[141] S. Lany, Band-structure calculations for the 3 d transition metal oxides in G W. Phys. Rev. B 87 (2013) https://doi.org/10.1103/PhysRevB.87.085112.

[142] P. Wang, X. Zhao, B. Li, ZnO-coated CuO nanowire arrays: fabrications, optoelectronic properties, and photovoltaic applications. Opt. Express. 19 (2011) 11271, https://doi.org/10.1364/OE.19.011271.

[143] R. Bhardwaj, R. Barman, D. Kaur, Improved photovoltaic effect in CuO/$Zn_{1-x}Mg_xO$ heterojunction solar cell by pulsed laser deposition. Mater. Lett. 185 (2016) 230–234, https://doi.org/10.1016/j.matlet.2016.08.092.

[144] L. Leontie, M. Caraman, A. Visinoiu, G.I. Rusu, On the optical properties of bismuth oxide thin films prepared by pulsed laser deposition. Thin Solid Films 473 (2005) 230–235, https://doi.org/10.1016/j.tsf.2004.07.061.

[145] J. Morasch, S. Li, J. Brötz, W. Jaegermann, A. Klein, Reactively magnetron sputtered Bi_2O_3 thin films: analysis of structure, optoelectronic, interface, and photovoltaic properties: Bi_2O_3 thin films: structure, optoelectronic, interface, and photovoltaic properties. Phys. Status Solidi A 211 (2014) 93–100, https://doi.org/10.1002/pssa.201330216.

[146] L. Leontie, M. Caraman, M. Alexe, C. Harnagea, Structural and optical characteristics of bismuth oxide thin films. Surf. Sci. 507–510 (2002) 480–485, https://doi.org/10.1016/S0039-6028(02)01289-X.

[147] H.T. Fan, X.M. Teng, S.S. Pan, C. Ye, G.H. Li, L.D. Zhang, Optical properties of δ-Bi_2O_3 thin films grown by reactive sputtering. Appl. Phys. Lett. 87 (2005) 231916, https://doi.org/10.1063/1.2136351.

[148] Q.-Y. Li, Z.-Y. Zhao, Interfacial properties of Bi_2O_3 homo-junction from first-principles calculations. Phys. Lett. A 379 (2015) 2766–2771, https://doi.org/10.1016/j.physleta.2015.08.002.

[149] H. Gobrecht, S. Seeck, H.-E. Bergt, A. Märtens, K. Kossmann, Investigations on evaporated films of bismuth oxide. II. Determination of type of conductivity and photoconductivity measurements on doped and undoped layers. Phys. Status Solidi B 34 (1969) 569–576, https://doi.org/10.1002/pssb.19690340217.

[150] J. Hou, C. Yang, Z. Wang, W. Zhou, S. Jiao, H. Zhu, In situ synthesis of α-β phase heterojunction on Bi_2O_3 nanowires with exceptional visible-light photocatalytic performance. Appl. Catal. B Environ. 142–143 (2013) 504–511, https://doi.org/10.1016/j.apcatb.2013.05.050.

[151] T.P. Gujar, V.R. Shinde, C.D. Lokhande, R.S. Mane, S.-H. Han, Bismuth oxide thin films prepared by chemical bath deposition (CBD) method: annealing effect. Appl. Surf. Sci. 250 (2005) 161–167, https://doi.org/10.1016/j.apsusc.2004.12.050.

[152] V. Dolocan, Transmission spectra of bismuth trioxide thin films. Appl. Phys. 16 (1978) 405–407, https://doi.org/10.1007/BF00885866.

[153] R. Mansfield, The electrical properties of bismuth oxide. Proc. Phys. Soc. Sect. B 62 (1949) 476–483, https://doi.org/10.1088/0370-1301/62/8/302.

[154] R.A. Evarestov, V.A. Veryazov, The electronic structure of crystalline lead oxides. I. Crystal structure and LUC-CNDO calculations. Phys. Status Solidi B 165 (1991) 401–410, https://doi.org/10.1002/pssb.2221650210.

[155] H.J. Terpstra, R.A. De Groot, C. Haas, The electronic structure of the mixed valence compound Pb_3O_4. J. Phys. Chem. Solids 58 (1997) 561–566, https://doi.org/10.1016/S0022-3697(96)00165-5.

[156] L.M. Droessler, H.E. Assender, A.A.R. Watt, Thermally deposited lead oxides for thin film photovoltaics. Mater. Lett. 71 (2012) 51–53, https://doi.org/10.1016/j.matlet.2011.12.027.

[157] D. Barreca, C. Massignan, S. Daolio, M. Fabrizio, C. Piccirillo, L. Armelao, E. Tondello, Composition and microstructure of cobalt oxide thin films obtained from a novel cobalt(II) precursor by chemical vapor deposition. Chem. Mater. 13 (2001) 588–593, https://doi.org/10.1021/cm001041x.

[158] Z.-X. Shen, J.W. Allen, P.A.P. Lindberg, D.S. Dessau, B.O. Wells, A. Borg, W. Ellis, J.S. Kang, S.-J. Oh, I. Lindau, W.E. Spicer, Photoemission study of CoO. Phys. Rev. B 42 (1990) 1817–1828, https://doi.org/10.1103/PhysRevB.42.1817.

[159] C.-S. Cheng, M. Serizawa, H. Sakata, T. Hirayama, Electrical conductivity of Co_3O_4 films prepared by chemical vapour deposition. Mater. Chem. Phys. 53 (1998) 225–230, https://doi.org/10.1016/S0254-0584(98)00044-3.

[160] J.G. Cook, M.P. van der Meer, The optical properties of sputtered Co_3O_4 films. Thin Solid Films 144 (1986) 165–176, https://doi.org/10.1016/0040-6090(86)90409-8.

[161] P.R. Athey, Optical properties of cobalt oxide films deposited by spray pyrolysis. J. Vac. Sci. Technol. Vac. Surf. Films 14 (1996) 685, https://doi.org/10.1116/1.580372.

[162] B. Kupfer, K. Majhi, D.A. Keller, Y. Bouhadana, S. Rühle, H.N. Barad, A.Y. Anderson, A. Zaban, Thin film Co_3O_4/TiO_2 heterojunction solar cells. Adv. Energy Mater. 5 (2015) 1401007https://doi.org/10.1002/aenm.201401007.

[163] K. Majhi, L. Bertoluzzi, D.A. Keller, H.-N. Barad, A. Ginsburg, A.Y. Anderson, R. Vidal, P. Lopez-Varo, I. Mora-Sero, J. Bisquert, A. Zaban, Co_3O_4 based all-oxide PV: a numerical simulation analyzed combinatorial material science study. J. Phys. Chem. C 120 (2016) 9053–9060, https://doi.org/10.1021/acs.jpcc.6b01164.

[164] T. Lindgren, L. Vayssieres, H. Wang, S.E. Lindquist, Photo-oxidation of water at hematite electrodes, in: A.I. Kokorin, D. Bahnemann (Eds.), Chemical Physics of Nanostructured Semiconductors, VSP, Utrecht, Boston, 2003, pp. 83–110 (Chapter 3).

[165] R.L. Kurtz, V.E. Henrich, Surface electronic structure and chemisorption on corundum transition-metal oxides: α-Fe_2O_3. Phys. Rev. B 36 (1987) 3413–3421, https://doi.org/10.1103/PhysRevB.36.3413.

[166] M. Catti, G. Valerio, R. Dovesi, Theoretical study of electronic, magnetic, and structural properties of α-Fe_2O_3 (hematite). Phys. Rev. B 51 (1995) 7441–7450, https://doi.org/10.1103/PhysRevB.51.7441.

[167] R.F.G. Gardner, F. Sweett, D.W. Tanner, The electrical properties of alpha ferric oxide-II. J. Phys. Chem. Solids 24 (1963) 1183–1196, https://doi.org/10.1016/0022-3697(63)90235-X.

[168] L.A. Marusak, R. Messier, W.B. White, Optical absorption spectrum of hematite, α-Fe_2O_3 near IR to UV. J. Phys. Chem. Solids 41 (1980) 981–984, https://doi.org/10.1016/0022-3697(80)90105-5.

[169] G. Dräger, W. Czolbe, J.A. Leiro, High-energy-spectroscopy studies of a charge-transfer insulator: X-ray spectra of α-Fe_2O_3. Phys. Rev. B 45 (1992) 8283–8287, https://doi.org/10.1103/PhysRevB.45.8283.

[170] Y. Ma, P.D. Johnson, N. Wassdahl, J. Guo, P. Skytt, J. Nordgren, S.D. Kevan, J.-E. Rubensson, T. Böske, W. Eberhardt, Electronic structures of α-Fe_2O_3 and Fe_3O_4 from O *K*-edge absorption and emission spectroscopy. Phys. Rev. B 48 (1993) 2109–2111, https://doi.org/10.1103/PhysRevB.48.2109.

[171] Z.D. Pozun, G. Henkelman, Hybrid density functional theory band structure engineering in hematite. J. Chem. Phys. 134 (2011) 224706, https://doi.org/10.1063/1.3598947.

[172] S. Somekawa, Y. Kusumoto, M. Abdulla-Al-Mamun, M. Muruganandham, Y. Horie, Wet-type Fe_2O_3 solar cells based on Fe_2O_3 films prepared by laser ablation: drastic temperature effect. Electrochem. Commun. 11 (2009) 2150–2152, https://doi.org/10.1016/j.elecom.2009.09.017.

[173] S. Rühle, A.Y. Anderson, H.-N. Barad, B. Kupfer, Y. Bouhadana, E. Rosh-Hodesh, A. Zaban, All-oxide photovoltaics. J. Phys. Chem. Lett. 3 (2012) 3755–3764, https://doi.org/10.1021/jz3017039.

[173a] D. Tiwari, D.J. Fermin, T.K. Chaudhuri, A. Ray, Solution processed bismuth ferrite thin films for all-oxide solar photovoltaics. J. Phys. Chem. C. 119 (2015) 5872–5877, https://doi.org/10.1021/jp512821a.

[174] J. Seidel, D. Fu, S.-Y. Yang, E. Alarcón-Lladó, J. Wu, R. Ramesh, J.W. Ager, Efficient photovoltaic current generation at ferroelectric domain walls. Phys. Rev. Lett. 107 (2011) https://doi.org/10.1103/PhysRevLett.107.126805.

[175] S.Y. Yang, J. Seidel, S.J. Byrnes, P. Shafer, C.-H. Yang, M.D. Rossell, P. Yu, Y.-H. Chu, J.F. Scott, J.W. Ager, L.W. Martin, R. Ramesh, Above-bandgap voltages from ferroelectric photovoltaic devices. Nat. Nanotechnol. 5 (2010) 143–147, https://doi.org/10.1038/nnano.2009.451.

[175a] A.J. Hauser, J. Zhang, L. Mier, R.A. Ricciardo, P.M. Woodward, T.L. Gustafson, L.J. Brillson, F.Y. Yang, Characterization of electronic structure and defect states of thin epitaxial $BiFeO_3$ films by UV-visible absorption and cathodoluminescence spectroscopies. Appl. Phys. Lett. 92 (2008) 222901, https://doi.org/10.1063/1.2939101.

[175b] T. Choi, S. Lee, Y.J. Choi, V. Kiryukhin, S.-W. Cheong, Switchable ferroelectric diode and photovoltaic effect in $BiFeO_3$. Science 324 (2009) 63–66, https://doi.org/10.1126/science.1168636.

[176] F. Zheng, Y. Xin, W. Huang, J. Zhang, X. Wang, M. Shen, W. Dong, L. Fang, Y. Bai, X. Shen, J. Hao, Above 1% efficiency of a ferroelectric solar cell based on the $Pb(Zr,Ti)O_3$ film. J. Mater. Chem. A 2 (2014) 1363–1368, https://doi.org/10.1039/C3TA13724D.

[177] R. Nechache, C. Harnagea, S. Li, L. Cardenas, W. Huang, J. Chakrabartty, F. Rosei, Band-gap tuning of multiferroic oxide solar cells. Nat. Photonics 9 (2014) 61–67, https://doi.org/10.1038/nphoton.2014.255.